Structure-Property Evaluation of CrN Coatings Developed for BUE Dominated High-Speed Machining Applications

Structure-Property evaluation of CrN Coatings Developed for BUE Dominated High-Speed Machining Applications

By

Shahana Akter

A Thesis Submitted to the School of Graduate Studies in Partial Fulfillment of the Requirements for the Degree Master of Applied Science

McMaster University, Hamilton, Ontario, Canada

Master of Applied Science (2023) McMaster University

(Department of Mechanical Engineering) Hamilton, Ontario, Canada

TITLE: Structure-Property Evaluation of CrN Coatings Developed for BUE Dominated High-Speed Machining Applications

AUTHOR: Shahana Akter

B.Sc. (Industrial and Production Engineering)

Bangladesh University of Engineering and Technology, Dhaka, Bangladesh.

SUPERVISOR: Dr. Stephen C. Veldhuis

NUMBER OF PAGES: xv, 87

LAY ABSTRACT

Coating properties such as hardness, residual stress, adhesive behaviour, elastic modulus, and roughness significantly affect tool performance and wear patterns, besides machining parameters and conditions. This research focuses on CrN coatings deposited by PVD cathodic arc deposition, adjusting the N_2 gas pressure while keeping bias voltage constant. The research investigates and illustrates that CrN coatings can be specifically tailored (by adjusting the N_2 gas pressure) to possess unique mechanical, and tribological properties that ameliorate machining performance in scenarios involving BUE formation. Three CrN coatings were deposited using the PVD technique by varying the N_2 gas pressure. A thorough coating characterization was conducted for each of three in-house deposited coatings and one commercially available coating. The wear behaviour of different CrN-coated WC tools was evaluated during dry finish turning of SS 304 to identify the best-performing coating. Lastly, high-temperature coating characterization was performed up to 450 ˚C for one in-house deposited coating (nitrogen gas pressure of 4 Pa, bias voltage of -50 V) and one commercial coating. The results showed that a coating that has low H/E ratio (without compromising elastic modulus), high plasticity index, high toughness, moderate residual stress and low roughness effectively minimizes issues related to sticking and BUE formation and retains coating properties at high temperatures.

ABSTRACT

Various nitrides, such as chromium nitride and titanium nitride, find extensive use in cutting tools, micromechanical devices, and medical implants due to their exceptional physical, mechanical, and chemical properties. These coatings exhibit superior hardness compared to high-speed steel and cemented carbide along with notable protective capabilities against corrosion and wear. These coatings have been successfully used to enhance the properties of cemented carbide and steel tools while safeguarding their surfaces. By adjusting deposition parameters like N_2 gas pressure, the properties of PVD coatings can be tailored to effectively withstand specific dominant wear modes during machining. The study investigates and demonstrates that CrN coatings can be specifically engineered to have distinct mechanical and tribological properties by adjusting the N_2 gas pressure, which enhances machining performance in cases where BUE formation occurs. A comprehensive coating characterization was conducted for each CrN coating studied. Wear performance assessments of the various CrN-coated WC tools were carried out during dry finish turning of SS 304. Additionally, high-temperature coating characterization was performed for the best-performing in-house deposited coating (nitrogen gas pressure of 4 Pa, bias voltage of -50 V) and a commercial coating, up to 450°C. The results highlighted the influence of N_2 gas pressure on the structural, mechanical, and tribological properties of CrN coatings. The findings indicate that coatings with a comparatively low H/E ratio (while maintaining higher elastic modulus values), low roughness, moderate residual

stress, high plasticity index, and high toughness exhibited superior performance when machining sticky materials and in high-temperature applications prone to adhesive wear and built-up edge (BUE) formation. Furthermore, high-temperature studies confirmed that the in-house coating retained a low H/E ratio, high plasticity index, high toughness, and low roughness, without compromising the hardness or elastic modulus values. In contrast, the commercial coating failed to retain its properties at higher temperatures. These high-temperature studies provide valuable insights for selecting CrN coatings tailored for machining materials that tend to adhere to the cutting tool and for high-temperature applications.

ACKNOWLEDGEMENTS

Throughout the completion of my M.A.Sc. thesis, I have received tremendous support and assistance, for which I am extremely grateful. First and foremost, I want to thank my supervisor, Dr. Stephen C. Veldhuis, for his guidance, and expertise. Under his mentorship, I have had the opportunity to learn from various projects which enhanced my understanding. I am also very grateful to my committee members, Dr. Maryam Aramesh and Dr. Fengjun Yan, for their insightful remarks and advice during this research.

I would also like to express my heartfelt gratitude to all my mentors, colleagues, and friends at the McMaster Manufacturing Research Institute (MMRI), especially Dr. Bipasha Bose and Dr. Mohammad Shariful Islam Chowdhury, for their constant support and guidance throughout this journey. Additionally, I am also thankful to Dr. Jose Mario DePaiva, whose advice and friendship have been invaluable during this research. My colleagues immense support helps me going through this journey. The knowledge and experience I gained throughout the years will be valued and cherished forever.

Finally, I thank my husband, Salman Buksh Sookran, and both sides of my family for their immense support and understanding. No words can express how obligated I am for their unending love, support, and sacrifice.

I also acknowledge the support of the Natural Sciences and Engineering Research Council of Canada (NSERC) for funding this research under the CANRIMT Strategic Research Network Grant NETGP 479639-15.

Contents

List of Figures

List of Tables

Notation and Abbreviations

CrN	Chromium Nitride
BUE	Built-Up Edge
AFM	Atomic Force Microscope
PVD	Physical Vapour Deposition
FIB	Focused Ion Beam
SEM	Scanning Electron Microscopy
EDS	Energy-Dispersive Spectrometry
XRD	X-Ray Diffraction
SS	Stainless Steel
WC	Cemented Carbide
DOC	Depth of Cut
RT	Room-Temperature
E	Elastic Modulus
H	Hardness
PI	Plasticity Index
CCR	Chip Compression Ratio
SA	Shear Angle

Chapter 1 – INTRODUCTION

1.1 Research Background and Motivation

Self-adaptive PVD coatings are used nowadays in many machining applications where adhesion-related problems predominate. For machining applications that involve titanium machining, stainless steel machining, or the stamping operation, one of the main drawbacks is the tendency for the work material to stick to the tool body. Such intensive adhesion results in built-up-edge (BUE) formation, and, as BUE is an unsteady structure, it can take a big chunk of tool material with it when it breaks. Because BUE formation is unavoidable in machining, reducing BUE formation is necessary for better tool performance and a smoother surface finish. To limit BUE generation, the properties of a coating need to be modified since it is primarily the properties that dictate the performance of a PVD coating. CrN coatings have been found to outperform other coatings in machining applications where BUE generation is dominant. Their chemical stability, excellent oxidation, and corrosion resistance, low coefficient of friction and enhanced toughness, play a significant role in machining sticky materials, as they help to reduce material adhesion. To attain these properties and reduce BUE, a certain combination of hardness, elastic modulus, H/E ratio, and plasticity index is required in a coating [1], [2].

Stainless steel is one of the most widely used metals not only in the manufacturing industry but also in most chemical and food processing

industries [3]. Out of all the stainless steel, SS 304 is used the most in building materials, medical equipment, aerospace, ship parts, and vehicle accessories. Several studies have been conducted for machining SS using cemented WC tools, high-speed steel (HSS) tools, diamond tools and ceramic tools. For machining stainless steels, cemented carbide tools are considered the most suitable commercially available tool material due to their ideal combination of high elastic modulus, resistance to thermal shock, abrasion resistance, resistance to corrosion, and mechanical impact strength [4], [5]. When working with SS 304, due to its machining restrictions in terms of adhesion wear, poor tensile strength, chemical affinity, and built-up edge, some irregular wear is observable on the tool surface.

In the manufacturing industry, vapour deposition techniques such as physical vapour deposition (PVD) and chemical vapour deposition (CVD) are frequently used to enhance productivity, safeguard tools, and improve tool life and performance. Hard transition metal nitride coatings produced by PVD cathodic arc plasma deposition have been employed successfully in many industrial applications, compared to CVD [6]–[8]. Due to its capability for fast deposition speeds and superior adherence of the coating to the surface, the cathodic arc process has been gaining popularity [9]. In the machining process, tool wear is unavoidable and due to this wear overall productivity, product quality, and dimensional accuracy are affected. Therefore, it is very important to reduce tool wear and to improve productivity and reduce tool wear rates. Tool coatings

are widely used in almost all machining applications. To design coatings with advantageous properties, various studies have attempted to comprehend the deposition process for CrN coatings as CrN forms a Cr_2O_3 tribo-film with thermal barrier characteristics [10].

Alongside other parameters like reactive gas pressure, bias voltage, deposition temperature, and table rotation speed, nitrogen gas pressure plays a vital role in depositing CrN thin films because it directly affects the formation of the main structure of the material [11]. Modifying the aforementioned parameters influences ion bombardment energy, considered as most crucial deposition variables that define coating features including residual stress, structure, and texture [12]. Previous research has shown that a relatively high nitrogen pressure results in less compressive residual stress than is seen at lower pressures. As interfacial stresses are high in higher compressive residual stress, the adhesion between the coating/substrate reduces, sometimes resulting in coating failure and spallation [13]. Another study found that nitrogen pressure can alter properties including structure, phase orientation, grain size, and defects; those properties can directly influence elastic modulus, coating's adhesion behavior, and hardness [6]. Besides these, nitrogen gas pressure can influence coating's chemical composition, which affects other characteristics like hot hardness and oxidation resistance [14], [15]. Therefore, a coating's properties, such as its microstructure, hardness, elastic modulus, residual stress, and adhesion, can be modified to achieve desired properties by changing those deposition parameters [16]–[19] for

a machining application where machining performance is dominated by a specific wear mode [6]. Previous researchers showed that, when the main aim is to reduce BUE formation, it is necessary for a CrN coating to have an optimum combination of micro-mechanical properties—a combination of a low H/E ratio, high toughness, low roughness, and high plasticity index—which is attainable by changing the deposition parameters [1], [2].

To the author's knowledge, no prior study has been conducted investigating the effect of N_2 gas pressure on CrN coatings, relating those properties to suitability for a particular application, and studying high-temperature effects on coating properties. Therefore, an in-depth characterization has been done to analyze the structural, mechanical and tribological properties of in-house deposited chromium nitride coatings and to compare them with a commercially available coating, providing valuable insights into finding the best deposition conditions to reduce built-up edge formation. Dry high-speed finish turning of SS 304 was conducted to identify the best coating that helps to minimize build-up edge and high-temperature studies were conducted for two coatings to figure out the effects of the structural, mechanical, and tribological properties of the coatings.

1.2 Research Objective

The primary objective of this study is to determine the essential properties of a CrN coating that contribute to enhanced tool performance against BUE formation and to identify how to achieve and/or manipulate these properties depending on the end application. The research goals of this study are as follows:

1. Investigate the influence of N_2 gas pressure on coating properties: Examine how variations in the N_2 gas pressure impact the properties of the coating.
2. Analyze structural, mechanical, and tribological Properties: Identify the structural, mechanical, and tribological properties of a coating tailored for a specific application by adjusting the N_2 gas pressure. Compare these properties with those of an existing commercial CrN coating.
3. Compare the tool performance of coated and uncoated CrN tools: Compare the performance of coated and uncoated CrN tools to determine the most suitable coating for machining adhesive materials.
4. Conduct high-temperature studies up to 450°C: Perform high-temperature investigations on two coatings—the top-performing in-house deposited coating and the commercial coating. Explore the impact of elevated temperatures (up to 450°C) on coating's structural, mechanical, and tribological properties.

By addressing these research objectives, this study aims to enhance our understanding of coatings' behaviour and performance under various conditions, contributing to the advancement of machining technologies and material processing.

1.3 Thesis Outline

This thesis is structured into five chapters. The outline is summarized below:

CHAPTER 1: INTRODUCTION – An overview of the research background along with the motivation and research objectives of this work are outlined in this chapter.

CHAPTER 2: LITERATURE REVIEW – To provide a thorough understanding of the research area pursued in this thesis, this chapter imparts a comprehensive synopsis of machining, tool wear and mechanisms, tool coatings, self-adaptive PVD coatings, the effect of deposition parameters, properties of, and challenges of machining stainless steel.

CHAPTER 3: EXPERIMENTAL PROCEDURE – Detailed information about the stratagem, experimental setups, workpiece and cutting tool materials, and experimental test parameters are presented in this chapter. The chapter is divided into three sections: Coating deposition; Experimental setup – Coating testing and characterization; and Experimental setup – Machining.

CHAPTER 4: RESULTS AND DISCUSSION – Detailed presentations of the study's findings are made in this chapter in three sections: Study A – Structural, mechanical and tribological properties of CrN coatings, Study B – Machining studies and Study C – Higher temperature studies.

CHAPTER 5: CONCLUSION and FUTURE WORK – This section provides a concise summary of the research, highlighting the important findings. Ideal deposition parameters for machining sticky materials are drawn from the study’s

outcomes. In addition, based on the findings of this study, recommendations are provided for future research.

Chapter 2 - LITERATURE REVIEW

2.1 Machining

To achieve a desired geometry, numerous metal removal processes are done on a block of material, and the material is removed in the form of chips in machining or metal cutting. The most common and widely used machining operations are turning, milling and drilling. A cross-sectional view of the machining process is shown in Figure 2.1.

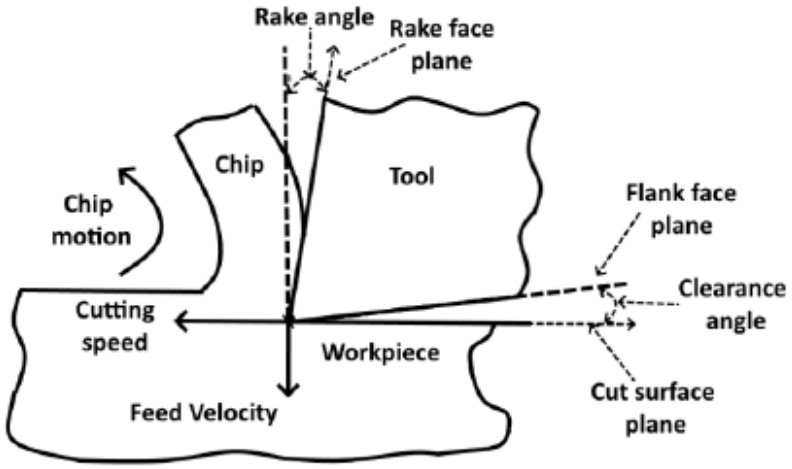

Figure 2.1 Machining process (cross-sectional view)

2.2 Tool Wear Modes and Tool Wear Mechanisms

During cutting, the shape of the tool can change from its original shape due to deformation or gradual loss of material. This phenomenon is called tool wear [20]. In machining, tool wear is unavoidable and affects overall productivity, product quality, and dimensional accuracy. Therefore, in any machining process, it is very important to reduce tool wear.

Tool wear occurs as a result of high temperature, load, and friction between the cutting tool and the workpiece. As a result of tool wear, the outer surface of the tool initially deforms or becomes displaced, finally breaking the tool or removing a big chunk of material from the tool. Figure 2.2 illustrates different types of tool wear seen on tools during machining. There can be both gradual and drastic breakdowns in tool wear [21].

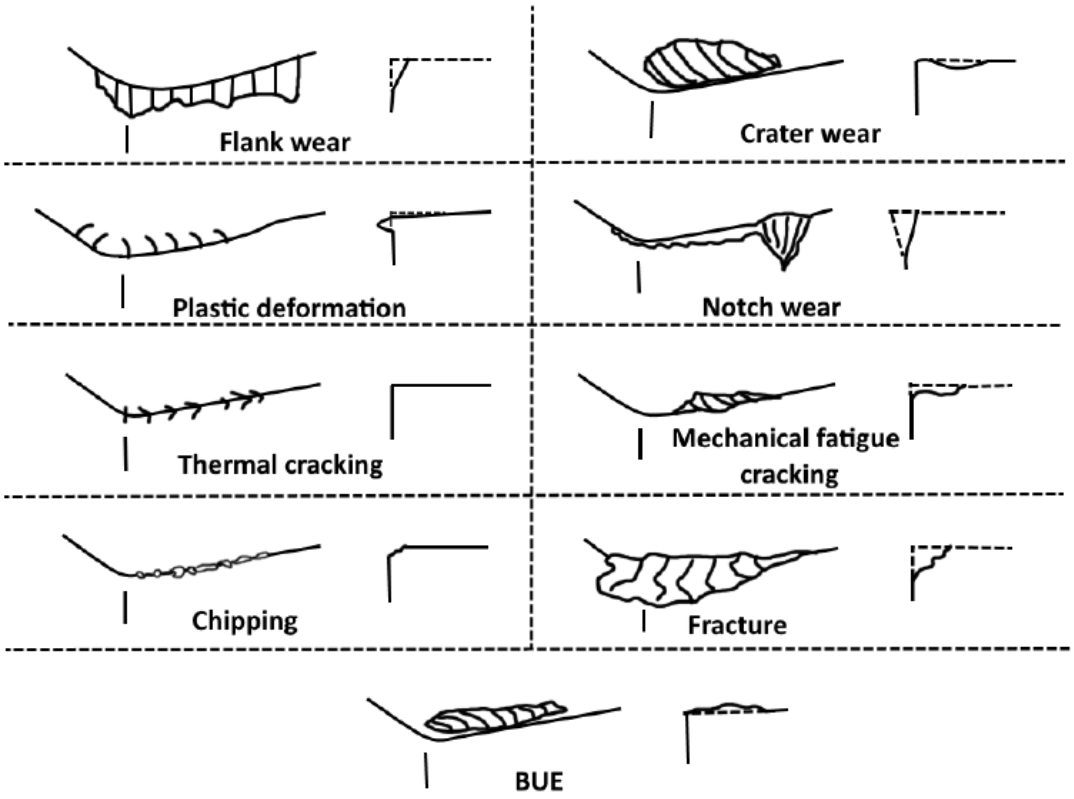

Figure 2. 1 Types of tool wear [22]

Gradual wear on tools appears as flank wear on the flank face, crater wear on the rake face, or notch wear usually on the flank face. It can develop by one or more combinations of the following wear mechanisms: diffusion, adhesion, abrasion, or plastic deformation. Sudden and unexpected loss or

breakage of material is a form of drastic breakdown which can appear through chipping, fracture, or thermal fatigue due to fluctuations in the temperature [23].

There are different types of tool wear such as BUE formation, flank wear, notch wear, crater wear, thermal and mechanical fatigue, fracture, plastic deformation, and chipping according to the ISO standard 3685:1993 [24]. Among these wears, the most common types of wear are flank wear and crater wear. Tool wear can be caused due to cutting speeds, depths of cut, and feed rates. For example, at high cutting speeds notch wear and diffusion wear were seen during machining [25].

2.3 Cutting Tool Coatings

The majority of the tools used in the machining sector nowadays are coated tools. A coating's primary goal is to improve the cutting tool's resistance to wear. In any machining operation, the highest temperature can be seen in the tool-chip interface due to friction. Coatings have been applied to minimize high cutting temperatures on the cutting tools. In order to understand the behaviour of a coating and how its use affects cutting temperature, detailed studies are required. Coatings should be designed to reduce friction, serve as a thermal barrier, supply wear resistance, and most importantly withstand severe machining conditions. Even at high temperatures and under heavy loads, it is necessary for a coating to maintain great adherence to the substrate of the cutting tool. The most commonly used coating techniques are PVD and CVD. Vapour deposition techniques (PVD and CVD) are frequently used in manufacturing the industry to enhance productivity,

safeguard tools, and improve tool life and performance. Hard transition metal nitride coatings produced by PVD cathodic arc plasma deposition have been employed successfully in many industrial applications, compared to CVD [6]–[8]. Due to the capability to achieve high deposition speed and superior adherence to the surface, the cathodic arc process has gained popularity [9].

2.3.1 PVD Coating

PVD is a vacuum coating process. Evaporation or sputtering is used in this procedure to physically remove the substance to be deposited from the target. The vapour particles inside the chamber get concentrated onto a substrate surface. On appropriately positioned parts, vapour particles are condensed, and thus create a film. In Figure 2.3, a schematic illustration of the PVD process is presented.

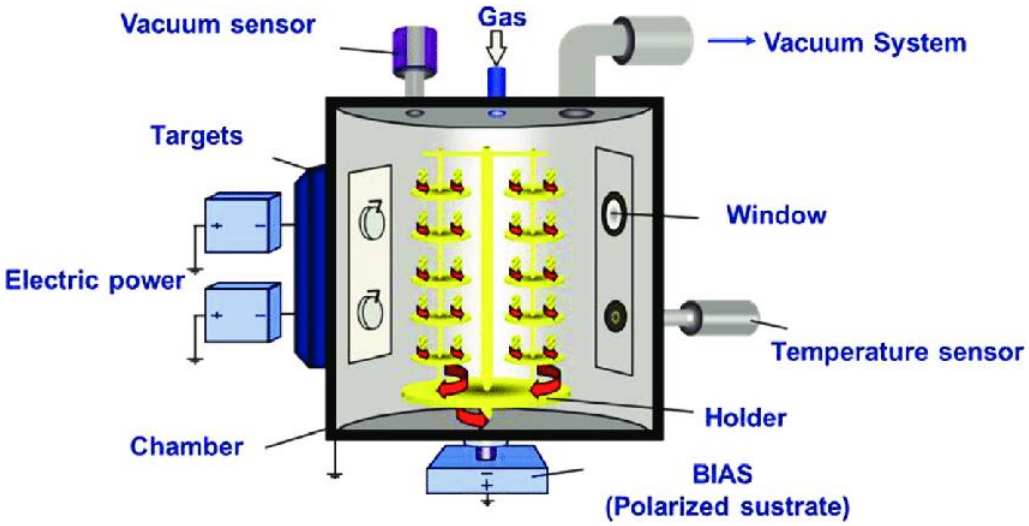

Figure 2.3 Schematic illustration of PVD process [26]

The average thickness range of coatings deposited using the PVD technique is a few nanometers to several microns. By employing a comparable source material or reactive gases like nitrogen, oxygen, or hydrocarbons carrying

desired reactants, chemical compounds can be deposited onto the desired surface by causing those sources to react with the metal inside the chamber [27]. PVD coating method produces sharp-coated edges. The resultant high intrinsic hardness and advantageous compressive stress of coatings applied via PVD prevent crack initiation. The ability to de-coat PVD-coated tools makes re-sharpening them considerably simpler and lowers production costs. Various PVD and CVD coatings have been utilized to improve the wear resistance of tools during stainless steel machining. It has been found that PVD-coated WC cutting tools exhibit longer tool life than CVD-coated WC cutting tools during the machining of super-duplex stainless steels [28].

Self-adaptive PVD coatings react to cutting conditions selectively. By interacting with their surroundings, self-adaptive coatings create advantageous tribo-films. As the coating system reacts with its environment (mostly oxygen), thin films called tribo-films form on the tool's worn surface or tool-workpiece interface. In comparison to the workpiece bulk material, these dynamic structures have diverse chemical compositions, tribological behaviours, and forms [29], [30].

According to the literature, self-adaptive PVD coatings can generate tribo-films at the tool-workpiece interface through interactions with the environment. These lubricious coatings could be applied to cutting tools to improve their wear performance during the machining of stainless steel.

2.3.2 CrN Coating

Various nitride coatings such as chromium nitride (CrN), titanium nitride

(TiN), zirconium nitride (ZrN) and so on are continuing to attract the attention of many researchers due to their mechanical, physical, chemical, and electrical properties. These coatings have superior hardness to that of high-speed steel and cemented carbide as well as demonstrated protective capabilities against corrosion and wear [8], [31]. These coatings have been used successfully to protect materials and improve certain properties of tools made of cemented carbides or steel. The CrN coating is one of the best among this group of coatings. CrN coatings have been developed for high-temperature wear applications, such as cutting tools or die-casting molds due to their distinct mechanical characteristics and oxidation resistance. Currently, CrN is one of the most widely employed hard coatings. Studies have shown that CrN coatings exhibit low thermal conductivity, excellent corrosion and wear resistance, and high microhardness [32]. CrN thin films also offer an ideal preference in corrosion and high-temperature applications, outperforming TiN thin films due to their lower temperature resistance [33]. In addition, a certain combination of properties of CrN coatings, such as a low H/E ratio (without compromising elastic modulus), low roughness, high plasticity index and high toughness performed better in reducing adhesion wear where BUE formation is predominant [1].

2.4 Deposition Parameter Effects on Coatings

The coating architecture, deposition technique, and process variables, such as the reactive gas pressure, bias voltage, deposition temperature, and table rotation speed, affect the mechanical properties and performance of PVD coatings

[6], [31], [34], [35]. Ion bombardment energy, one of the most important deposition variables that determines coating properties including structure, residual stress, and texture, is affected by modifying the aforesaid parameters [12]. Previous studies have demonstrated that increases in nitrogen gas pressure correspondingly reduce the amount of compressive residual stress. Higher compressive residual stress is associated with higher interfacial stresses, which reduces the adhesion between the coating/substrate system. In some cases, this can result in coating failure and spallation [13]. Another study stated that nitrogen pressure can change coating properties including structure, grain size, preferential orientation, and coating defects. These properties can have a direct impact on coating adhesion, elastic modulus, and hardness [6]. In addition to these, nitrogen pressure can modify a coating's composition, which affects other properties such as oxidation resistance and hot hardness [14], [15]. Therefore, by adjusting the deposition parameters, a coating's properties such as hardness, elastic modulus, microstructure, adhesion, and residual stress, can be modified to obtain desired attributes [16]–[19] for a machining application where a particular wear mode dominates machining performance [6]. Previous researchers have shown that an optimal combination of micromechanical properties such as a lower H/E ratio, higher toughness, lower roughness and higher plasticity index of CrN coatings, is necessary where BUE formation is predominant and which can be attainable by changing the deposition parameters [1], [2].

2.5 Stainless Steel

Stainless steels are mostly selected for their advantageous characteristics, such as their resistance to corrosion, excellent strength, high-temperature oxidation resistance, or cryogenic capabilities. About 18% chromium (Cr) is present in SS 304. As Cr enhances grain refinement, it helps to increase the hardness of steel without transforming the ductility. Furthermore, at high temperatures, SS 304's strength is also increased because of Cr content. At least 8% nickel (Ni) is present in SS 304 which contributes to improved toughness, especially at low temperatures, and diminishes scratches. Ni also helps SS 304 resist heat, which contributes to the material's low thermal conductivity [36], [37]. Due to the inability of the heat generated at the tool/chip/workpiece interfaces to be transmitted away from the edge of the tool, the temperature rises significantly, making SS304 difficult to machine. The temperature of the cutting tool might reach 1000 °C during machining because 80% of the heat produced is transmitted to the tool. This high-temperature results in the acceleration of tool wear through diffusion and oxidation [38]. Another challenge of machining SS 304 is its high strain hardening rate. As a result, more workpiece material adheres to the cutting tool causing BUE formation and producing unstable chips [39].

2.5.1 Machining Challenges of SS 304

2.5.1.1 Built-Up Edge

Due to high friction and pressure at the tool-workpiece interface material sticks to the rake face of the tool. As the material gets deposited and reaches a

critical amount, it starts to contribute to the cutting process. This welded material (BUE) causes dimensional inaccuracy and poor surface finish as the geometry of the tool changes. Eventually, a part of that welded material will detach during machining which may result in crater wear, as during the detachment a small portion of the tool may be carried away. During the turning of SS 304 using a WC P10 cemented carbide tool, it has been seen that with the increase in feed rate BUE builds up, but it diminishes with the increase in cutting speed [40].

2.5.1.2 Plastic Deformation

The machining of soft (Ductile) materials sometimes results in tool chipping and wear as the materials get plastically deformed past the yield point. As high temperatures result at the interface between tool and workpiece, the continuous chips stick to the tool. When the chips eventually split away, , they carry a small portion of the tool with them [41]. Sometimes these long continuous chips create a bird's nest which damages both the workpiece and the tool.

2.5.1.3 Thermal Conductivity

During machining, the highest temperature occurs at the tool-chip interface. The materials near the shear plane undergo plastic deformation and form chips that flow over the tool rake face. Near the secondary shear zone, however, the chips further experience plastic deformation which results in an increase in temperature at the tool-chip interface. Only a small portion of heat travels toward the workpiece due to the lower thermal conductivity of stainless steel. The temperature of the tool can rise to 1000˚C as almost 80% of the generated heat

gets passed to the tool. High temperatures cause oxidation and diffusion wear, resulting in rapid tool wear and shortening tool life [42].

2.5.1.4 Work Hardening

Work hardening of any material is undesirable. Heat generates between the cutting tool and workpiece and work hardening occurs when heat transfers to the workpiece material and leads to plastic deformation. Work hardening can cause both abrasive and notch wear. However, notch wear can also occur due to corrosion or other chemical processes [43].

2.5.2 Various Cutting Tool Materials

High-speed steel (HSS) has been widely used for machining various alloys. However, its use is limited by the tool's catastrophic failure, as chips become excessively hot above 45 m/min cutting speed. Researchers have found that high-speed steel tools fail due to fatigue failure and have a shorter tool life than cemented carbide tools [44].

Diamond tools such as cubic boron nitride (CBN), polycrystalline diamond (PCD), and natural diamond (ND) are used to machine various non-ferrous alloys due to their high hardness and dimensional stability. However, diamond tools are not suitable for machining stainless steel because of their strong carbon affinity. In addition, they are the most expensive cutting tools [45].

Ceramic tools are highly regarded for machining non-ferrous metal due to their chemical stability and low affinity. Moreover, they offer outstanding resistance to abrasion and crater wear as well as high-temperature compressive strength and

hardness. However, their application in machining steel alloys is limited due to their low fracture toughness, tensile strength, and thermal shock resistance [46], [47].

Cemented carbide tools are widely used for machining metal materials. Many researchers have used cemented carbide-coated tools during the machining of stainless steel. Ahmed et al. [48], studied the effect of BUE on the stable region of the tool life curve during the machining of SS 304 with an uncoated WC tool. The results revealed that as BUE formation increased, the tensile residual stress in the tool decreased. Xavior et al. [49], investigated the influence of different cutting fluids on tool wear and surface roughness during the turning process of SS 304 with a WC tool. Chandramohan [25] used the Taguchi method to find out the appropriate process parameters that helped to reduce surface roughness during dry machining of SS 304. However, obtaining low surface roughness during dry machining conditions remains a persistent challenge.

2.5.3 Dry High-Speed Machining

Within the manufacturing industry, there has recently been an increasing interest in green or dry manufacturing. This approach aims to reduce negative environmental effects while addressing occupational health and safety-related concerns. The primary benefits of dry machining include reduced air and water pollution, elimination of liquid residue on the workpiece that requires cleaning and elimination of additional costs associated with liquid disposal and cleaning agents. The intake of liquid lubricants and coolants may cause skin irritations and respiratory damage. Overall, dry machining reduces machining expenses by 16 –

20% [50], [51]. However, the disadvantages of dry machining include increased adhesion and friction between the tool-chip interface [52]. Tekiner and Yeşilyurt [40] conducted research to determine the optimal cutting conditions for machining SS 304 using acoustic emissions. Various combinations of cutting speed, depth-of-cut and feed rate were varied in the study using a WC tool. The data demonstrated that increasing cutting speed and feed rate result in a significant reduction in BUE formation.

To enhance the machinability of SS 304, numerous studies have been conducted using various cutting tools, coatings deposited by different deposition methods, and cutting conditions. In machining, achieving an acceptable surface quality is very challenging. A substantial amount of research has been conducted to improve the surface roughness by fine-tuning both the machining parameters and the machining conditions. Xavior et al. [49] investigated the tool wear and surface roughness of AISI 304 using different cutting fluids. Selvaraj and Chandramohan [53] used the Taguchi method to identify the optimal parameters for machining AISI 304 to reduce surface roughness. Despite these efforts, achieving minimal surface roughness during dry machining is still challenging.

2.5.4 Wear Performance - Coated Tools Used in Machining SS

In machining, flank wear is considered one of the most critical types of wear [54], drawing the attention of many researchers investigating its occurrence during stainless steel machining. According to current research, the use of PVD coatings on cutting tools reduces flank wear [55]. The enhanced performance of PVD

coatings is due to the formation of tribo-films that serve as a protective thermal barrier.

Adhesion is another wear mechanism commonly found while machining stainless steel. This leads to the formation of BUE, contributing to undesirable friction conditions at the tool-workpiece interface. Ciftci [56] investigated BUE generation using CVD coated carbide tools during the machining of AISI 316 and AISI 304 at cutting speeds of 120 m/min and 180 m/min. the results showed that at low speeds, the coated tool exhibited rapid tool wear along with occasional chipping, whereas at high speeds, the tool's cutting edge demonstrated less wear. The variance in performance can be ascribed to reduced adhesion between the cutting tool and BUE at higher cutting speeds.

2.6 Machining Parameters Selection

Figure 2.3 illustrates a summary of the literature about machining parameters. A machining condition for dry high-speed machining has been carefully chosen for the current study through a detailed analysis of the machining parameters available in the literature.

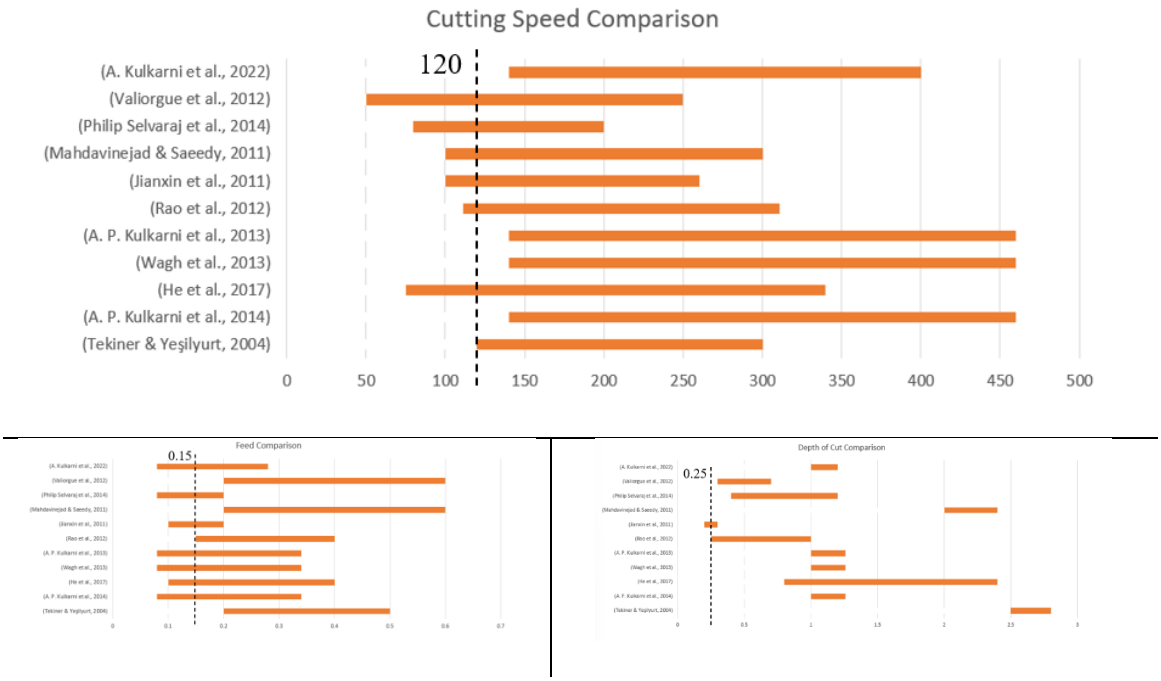

Figure 2. 2 Selection of machining parameters based on the literature

For machining SS 304, a speed of 120 m/min, feed rate of 0.15 mm/rev and depth of cut of 0.25 mm were chosen. No coolant was used during machining.

Chapter 3 – EXPERIMENTAL WORK

In this chapter, the experimental methodology is presented. The experimental setup was designed to investigate the effect of N_2 gas pressure on coating properties. The objective was to figure out the most effective combination of properties for mitigating the adhesive-related problem. Through a dry high-speed machining test, an investigation was conducted to determine if a certain combination of properties could reduce BUE formation and to identify the optimal deposition parameters. Lastly, high-temperature studies were performed using the best-performing in-house coating and the commercial coating. The goal was to investigate the effect of high temperatures on the coating properties.

In the first section, the deposition technique and procedure for the coating deposition are discussed.

Instruments and parameters used to analyze the microstructural, mechanical, and tribological properties of the coatings are discussed in the second section. The characterization data was collected to help figure out the optimal combination of properties for minimizing BUE formation. In this section, instruments and parameters used for high-temperature studies are also presented.

In the last section, machine information and cutting parameters are described for machining SS 304. Presented in this section is the procedure used for analyzing tool life performance, cutting force data, and tribological studies of the chips.

3.1 Coating Deposition

CrN coatings were deposited onto Kennametal CNGG432 and RNG45 tungsten carbide cutting inserts by arc evaporation using an AIP-S20 PVD coater (Kobelco, Japan) with a 100 mm-diameter Cr target (99.9% purity) at the McMaster Manufacturing Research Institute's PVD coating facility. The mirror-polished WC substrates were cleaned in acetone with an ultrasonic cleaner. The substrates were cleaned in-situ using argon ion etching with a substrate bias voltage of 400 V at a pressure of 1.33 Pa for 7.5 minutes after the pumping-down technique, which reached a pressure of 10 x 10^{-3} Pa. The Cr target was powered in arc mode. The temperature of the chamber was 500 °C during the deposition process. N_2 was used as the processing gas. The pressure of the N_2 gas varied while maintaining a bias voltage of -50V. Table 3.1 shows the nomenclature for the coatings and the variation in deposition parameters.

Table 3. 1 Variation of deposition parameters

Nitrogen gas pressure (Pa)	Bias voltage (V)	Temperature (˚C)	Arc Currents (A)	Rotation Speed (RPM)
1.33 (Coating A) 4 (Coating B) 5.5 (Coating C)	-50	500	150	5

3.2 Coating Testing and Characterization

The coatings were deposited on Kennametal CNGG432 and RNG45 tungsten carbide cutting inserts. The inserts were polished using an automatic

polisher before deposition. The flat, polished RNG45 inserts were used for the coating characterizations. Using the Calotest method, coating thickness was measured with a 25 mm steel ball. With a Helios 5 UC Dual Beam scanning electron microscope (SEM), optical examinations of the crystalline structures of the coatings' fracture sections were performed. An FEI Magellan 400 with SEM that was equipped with two Oxford Instrument X-Maxn 80 mm2 EDS detectors was used to perform and analyze composition measurements. Image J software was used to measure the area fraction of porosity and area fraction of macroparticle density.

An Anton Paar-NHT3 Nanoindentation Tester (Buchs, Switzerland) (Figure 3.1) was used to measure the coating's hardness and elastic modulus. For each insert, at room temperature with a Berkovich diamond indenter at a load of 40 mN 10 nanoindentations were done to measure the hardness and elastic modulus of the coating. During indentation, to avoid any substrate effect as well as to lower the impact of surface roughness, the penetration depth was kept at less than 10% of the total coating thickness.

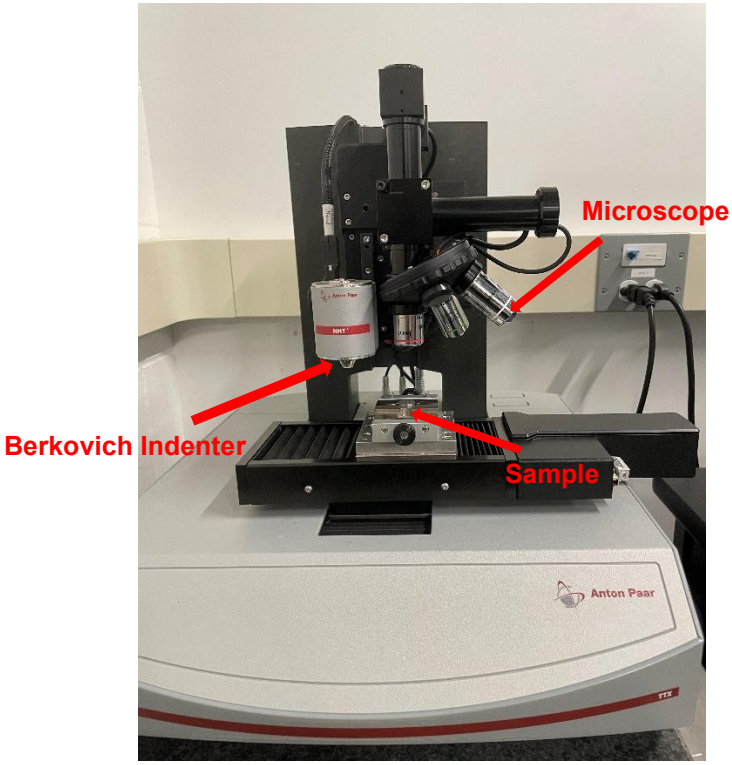

Figure 3.1 Experimental setup for the nano-indentation test

To study the failure behaviour of the coating, an Anton Paar-RST3 Revetest® Scratch Tester (Buchs, Switzerland) (Figure 3.2) was used under progressive loading. The tests were performed with a 100 µm end radii Rockwell diamond indenter, with loads increasing progressively from 0.5 N to 40 N for a scratch length of 3.5 mm. For high-temperature studies a 200 µm end radii Rockwell diamond indenter under a progressive load of 0.5 N to 150 N was used. At a 0.5 N load, pre- and post-topography scans were conducted. The scratching speed and loading rate were kept constant at 4.43 mm/min and 50 N/min, respectively. For each coating, the tests were iterated three times.

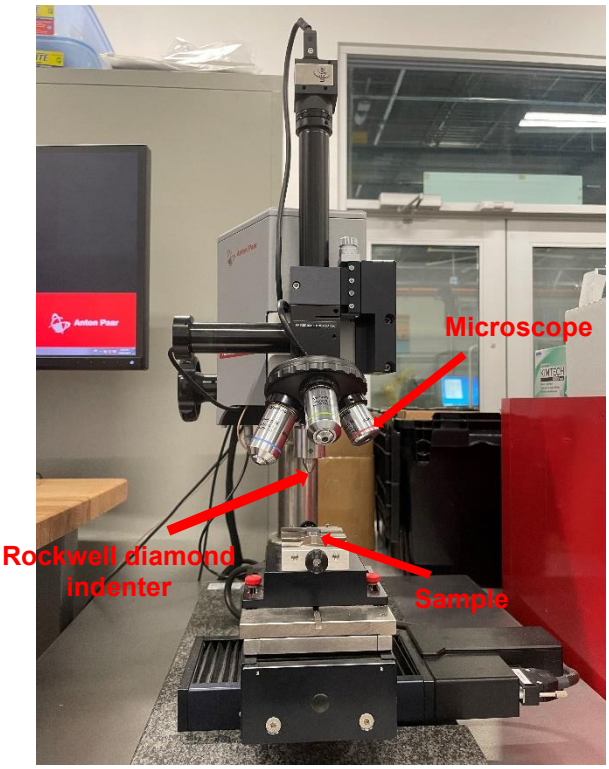

Figure 3.2 Experimental setup for the scratch test

An Anton Paar- TRB3 Pin-on-Disk tribometer (Figure 3.3) was used to measure the coefficient of friction of the coatings. All the tests were done with a 6 mm alumina ball where the normal load was 20 N, the total distance was 250 m, the amplitude was 4 mm, and the frequency was 8 Hz. With the help of an Alicona Infinite Focus G5 3D, provided by Alicona Manufacturing Inc. (Bartlett, IL, USA), the wear track profile was measured using a surface measurement module. The length of the wear track was measured using a Keyence optical microscope, model VHX-5000 Series, KEYENCE America (Elmwood Park, NJ, USA).

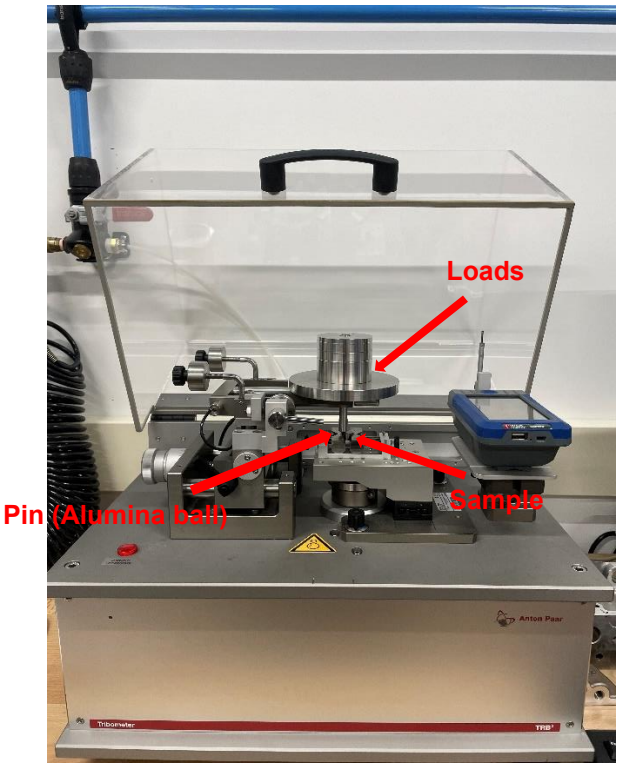

Figure 3.3 Experimental setup for measuring the coefficient of friction

A Durascan 50 5G (Figure 3.4) was used to measure the toughness of the coatings. The applied load was HV5 and the toughness values were calculated by the load and the total crack lengths (measured from the crack tip to the corner of each indent). The roughness measurements were performed on an Alicona Infinite Focus G5 3D surface measurement system (Alicona Manufacturing Inc., Bartlett, IL, USA). The scan area for measuring the roughness was approximately 1.6 mm x 1.6 mm and the magnification was 10 x. The measurements were taken three times and an average value was considered. Optical images of the coating surfaces were taken on a VHX-5000 Keyence optical microscope (KEYENCE Corporation of America, Itasca, IL, USA).

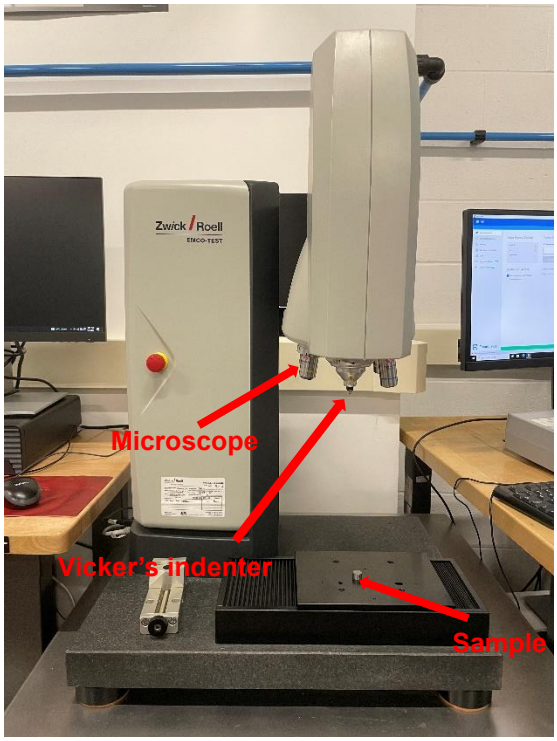

Figure 3.4 Experimental setup for measuring toughness

A Bruker D8-Discover equipped with a 2D detector VAATEC-500 was used to investigate the phase composition and crystal structure of the coatings. The radiation was Cu-Kα (1.540 Å) and the operating conditions were 40 kV and 40 mA. The software used for residual stress calculation was LEPTOS 7.8 and for phase identification, DIFFRAC.EVA V6.0. The grazing incidence diffraction method was used for phase identification and residual stress measurement. To identify the diffraction planes, a comprehensive scan was performed where the angular range was 10˚ to 90˚, using an incidence angle of 2˚.

The surface topography and morphology of CrN coatings were estimated with the help of an Anton Paar Tosca^{TM} 400 atomic force microscope (AFM) (Graz,

Australia) (Figure 3.5). For the scanning process, the tapping mode was used with a commercial silicon probe of 285 kHz resonant frequency and 42 N/m constant force. The scan area was 2 μm x 2 μm and the Tosca™ (version-7.4.8341) analysis software was employed for data analysis and image processing.

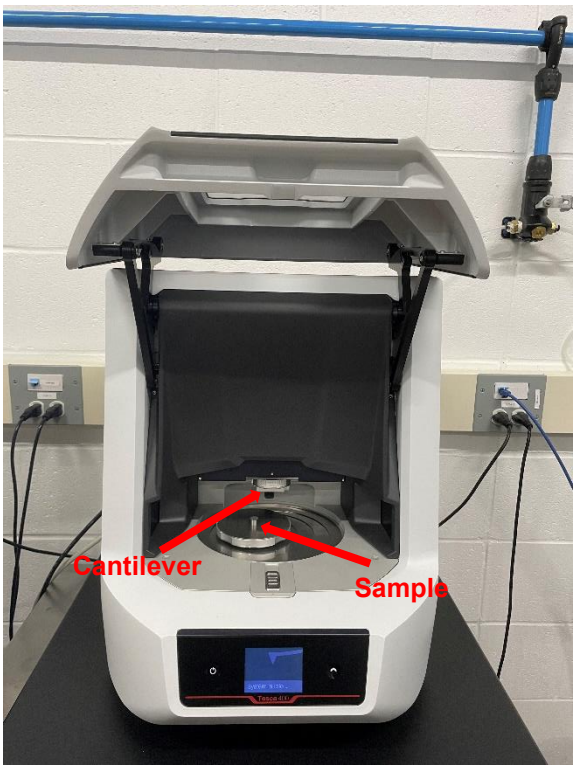

Figure 3.5 Experimental setup for measuring surface morphology and roughness

High-temperature studies were performed using a Nabertherm furnace. The samples were heated up to 450 ˚C using increments of 150 ˚C. For each temperature, a separate set of samples was used. The samples were held inside the furnace for one hour before being taken out to cool in the air. Once the samples were fully cooled down, tests were performed on them see how high temperatures affected the coating properties.

3.3 Machining

The coated tool wear characteristics were investigated using cutting tests. Dry high-speed turning tests were performed on a NAKAMURA SC450 turning machining centre (Nakamura company, Hakusan Ishikawa, Japan) using an MCLN-5° Kennametal KenlocTM tool holder. Figure 3.6 demonstrates the experimental setup for dry high-speed turning operation. CNGG432 carbide grade (WC, 6% Co) K313 inserts from Kennametal were used for dry finish-turning studies. A round bar (105 mm diameter by 250 mm length). of AISI 304 was investigated during machining.

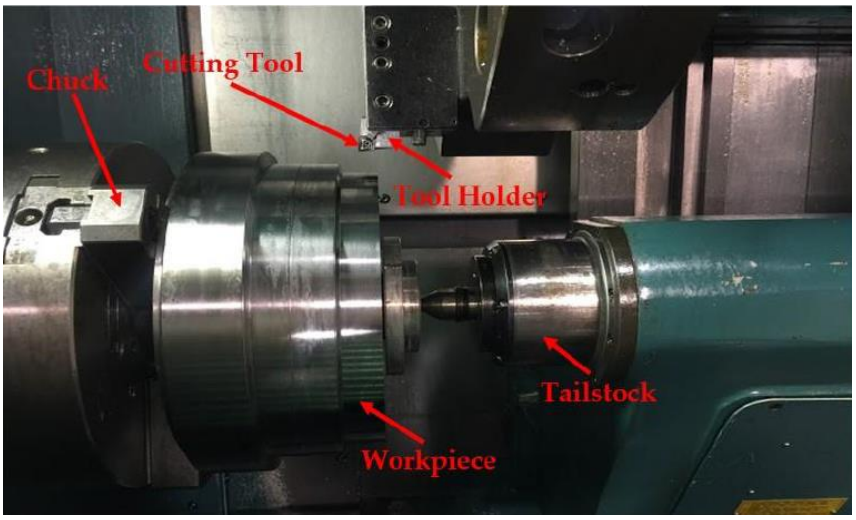

Figure 3.6 Emperical setup for dry high-speed turning

Table 3.2 illustrates the mechanical properties and chemical composition of SS 304 [14], and Table 3.3 summarizes the cutting parameters for the experiments. The cutting conditions were selected on the basis of the literature review and industrial recommendations.

Table 3. 2 Chemical composition and mechanical properties of stainless steel 304

Chemical Composition (%)						
C	Si	Mn	S	P	Cr	Fe
0.08	1.0 max	2.0 max	0.03 max	0.045 max	18-20	Balance
Mechanical Properties						
Yield strength	Tensile strength	Modulus of elasticity	Shear Modulus	Elongation	Poission's ratio	Hardness
215 MPa	505 MPa	193-200 Gpa	86 GPa	70%	0.29	123 HB

Table 3.3 Cutting parameters

Cutting data						
Machining Operation	Cutting tool substrates	Workpiece material	Speed, m/min	Feed, mm/rev	Depth of cut, mm	Coolant condition
Turing	Kennametal CNGG432	AISI 304	120	0.15	0.25	-

Progressive tool wear studies were conducted on Kennametal CNGG432 carbide grade (WC, 6% Co) K313 inserts under dry high-speed machining. The tool life was assessed by measuring the tool flank wear after each cutting pass. All the flank wear measurements were taken on a VHX-5000 Keyence optical microscope (KEYENCE Corporation of America, Itasca, IL, USA). According to the standard set out in ISO 3685:1993, the cutting tests were carried out until each tool achieved a maximum flank wear of 300 μm [24]. In addition to flank wear analysis, chip morphology analyses were performed on chips collected after roughly 10 m of cutting, using standard practices [57].

Volumetric wear measurements were performed on the worn tools at intervals of around 200 meters of cutting length. An Alicona Infinite Focus G5 3D surface measurement system (Alicona Manufacturing Inc., Bartlett, IL, USA) was

used for detailed inspections of the cutting inserts. The Alicona 3D optical system with focus-variation technology generated 3D topographical images of the inserts with color transition information and precisely measured the volumetric difference between each tool when new and worn using the Measure Suite module. A 3D volumetric dataset showing the cutting edge of each tool in its unused state was acquired as a reference before any cutting experiments were carried out. After approximately every 200 meters of cutting length, a 3D volumetric dataset of the same cutting edge on the used tool was acquired. By computing the volumetric difference between the worn tool and the reference dataset, the Measure Suite module aligned the two datasets and assessed the degree of crater wear and built-up volume on the cutting tools. Chip undersurface surface roughness measurements were taken with the Alicona Infinite Focus profile roughness module. Each evaluation was carried out three times, and an average reading was taken.

A Kistler Type 9129AA, a 3-component piezoelectric dynamometer, was used during machining to measure the resulting cutting forces. The sampling rate for data collection was 10 kHz. The LabAMP System developed by National Instruments (NI) was used for data processing. Subsequently, chip analysis was performed in accordance with M. Shaw [57]. The chips were collected after a cutting length of approximately 10 m. The scan area was approximately 3 mm x 3 mm for all the chips. The magnification was 10 x. The thicknesses were measured multiple times, and the average value was considered. The undersurface of the

chips was analyzed using an Alicona Infinite Focus G5 equipped with a profile roughness module.

Chapter 4 – RESULTS AND DISCUSSIONS

In this chapter, the experimental data and results are discussed. This chapter consists of three sections. In the first section, the structural, mechanical, and tribological analysis of the coating is presented. A detailed investigation was conducted, which is interpreted in this section, to identify the combination of properties that performs best in circumstances with adhesion-related problems. The second section demonstrates the machining results. By comparing the tool life performance, cutting force data, and chip analyses, a decision was made regarding the best-performing coating. Finally, the last section describes high-temperature study results for the best-performing coating (as derived from the machining results) and a commercial coating. This section pinpoints the effects of high temperatures on coating properties.

4.1 Coating Characterization

4.1.1 Microstructural Analysis

The in-house coatings were deposited at 1.33 Pa (Coating A), 4 Pa (Coating B) and 5.5 Pa (Coating C) nitrogen gas pressure. A minimum (1.33 Pa), average (4 Pa), and maximum (5.5 Pa) N_2 gas pressure were chosen: at lower nitrogen gas pressures, many particles failed to react adequately with the N ions prior to the deposition. As a result, the concentration of Cr ions became greater than the N ions in the coating [13]. If the nitrogen gas pressure is high, target poisoning might

occur where the target surface is coated with a nitride compound having a higher melting point compared to its original metallic form [3].

In order to evaluate coating's elemental compositions EDS was used. The elemental weight percentage (wt.%) for the coatings on the tungsten carbide inserts is represented in Table 4.1. The results indicate a comparable elemental composition for all the CrN coatings.

Table 4.1 Elemental compositions (wt.%) of all WC-coated inserts

	N	Cr
Coating A	17.9	82.09
Coating B	18.01	81.99
Coating C	17.8	82.19
Commercial	18.35	81.65

The X-ray diffraction patterns, presented in Figure 4.1 for all the CrN coatings, revealed that the coatings have Body Center Cubic (BCC) structures and display distinctive peaks at the (111), (200), (220), and (311) crystallographic planes.

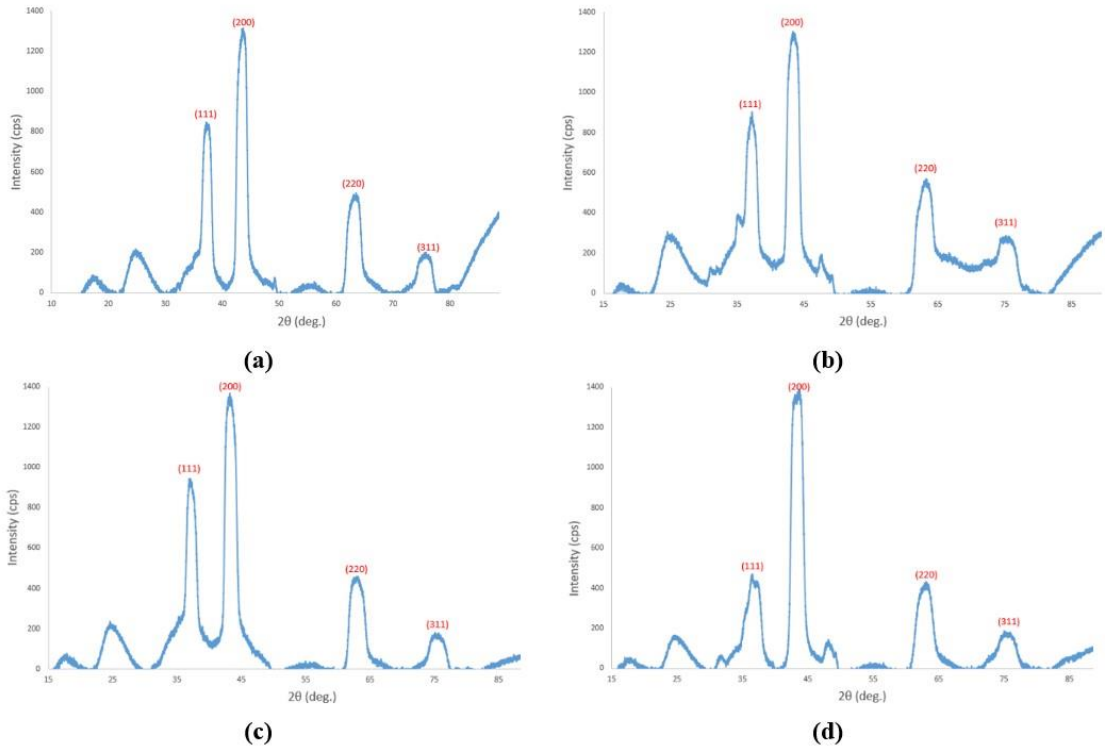

Figure 4.1 XRD patterns of the CrN coatings: (a) Coating A, (b) Coating B, (c) Coating C, and (d) Coating D

Every one of the CrN coatings exhibited a predominant crystallographic orientation along the (200) plane [58]. The in-house deposited and commercial coatings showed columnar structures as depicted in the coating FIB cross-section in Figure 4.2.

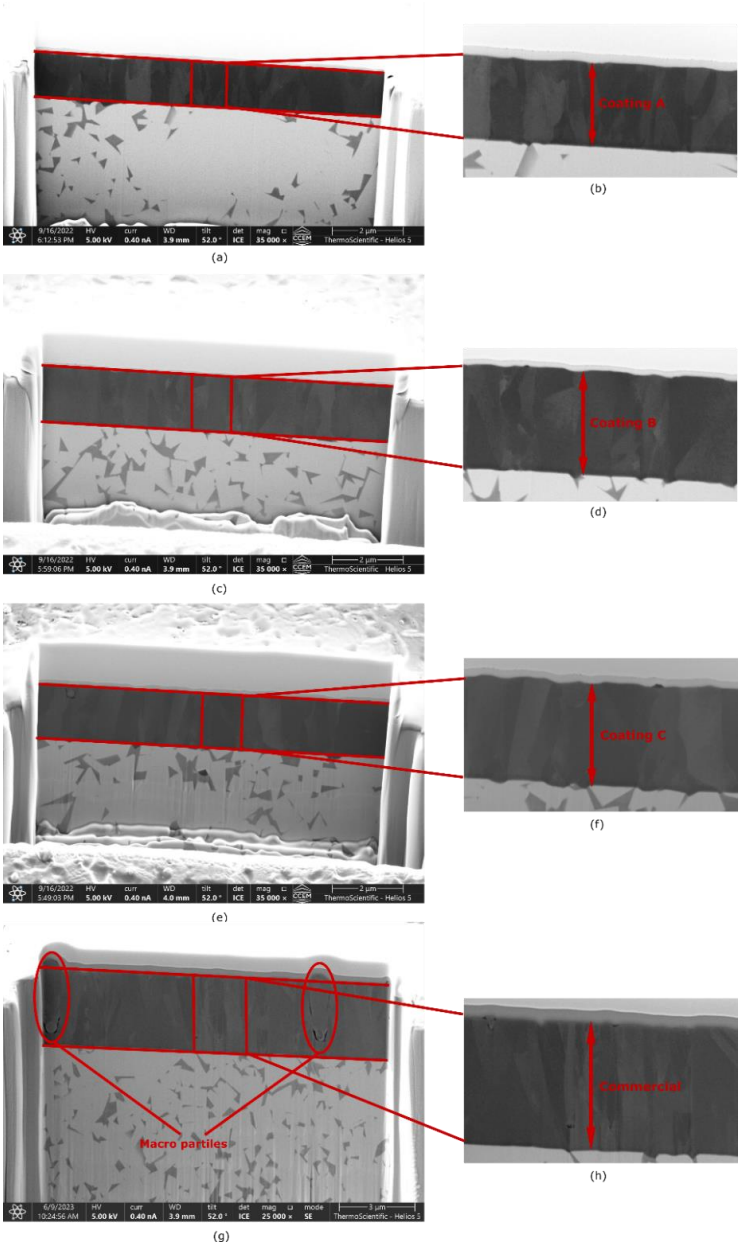

Figure 4.2 FIB cross-sections (SEM) of CrN coating showing coating structure and thickness as well as macroparticles in the commercial coating: (a,c,e,g) at 5000 x magnification; (b,d,f,h) at 20000 x magnification

It can be seen from Figure 4.2 that with an increase in N_2 pressure, the coatings exhibited columnar crystal growth. In Figure 4.2 (e,f), the columnar structure is more prominent [16]. During the nucleation process in PVD, the

presence of energetically strong crystallographic texture within a material occurs when grains with a favourable orientation expand outward and upward, resulting in columnar growth structures [59]. Although all the CrN coatings had similar compositions, the dissimilarity in the micro-mechanical properties, as depicted in Table 4.2, can be ascribed to variances in the coatings' structures, as shown in Figure 4.2. It has been seen in the literature that variations in column size as well as inter-column spacing and distribution can greatly influence the properties and performance of coatings, regardless of them having comparable compositions [60]–[62]. For example, when column boundaries are dense, the compressive stress and hardness of the material tend to increase [63].

Table 4.2 Micro-mechanical characteristics and residual stress values of CrN coatings

Nomenclature	**CrN Coating**			
	Coating A	**Coating B**	**Coating C**	**Commercial**
Thickness, µm	1.32±0.1	1.84±0.1	1.93±0.1	2.01±0.1
Hardness, GPa	21.7±2.4	19.1±0.44	17.4±1.7	18.7±3.6
Elastic Modulus, GPa	373.24±17.9	400.92±23.96	343.66±29.8	346.86±85.3
H/E Ratio	0.058±0.009	0.048±0.003	0.051±0.005	0.054±0.021
H^3/E^2 Ratio	0.073±0.03	0.043±0.005	0.044±0.01	0.055±0.073
Plasticity Index	0.53±0.03	0.61±0.02	0.58±0.04	0.53±1.35
Mean Coefficients of Friction, µ	0.34±0.02	0.15±0.04	0.25±0.04	0.43±0.03
Modified Palmqvist Toughness,	0.8±0.06	1.23±0.05	0.72±0.01	0.86±0.03

N/μm				
Roughness Sa, μm	0.16±0.19	0.12±0.15	0.14±0.17	0.24±0.38
Residual Stress, MPa	-1942.9±168.1	-761.5±153.7	-559.8±108.8	-538.9±117.0

With this in mind, the higher compressive stress and hardness levels observed in Coating A compared to the others (as stated in Table 4.2) can be attributed to its densely packed column boundaries. Many researchers have highlighted that the presence of macroparticle density [14] as well as porosity [64], [65] adversely affect a coating's micro-mechanical properties, topography, and performance, and as a result, it is generally preferred to minimize their presence. In Figure 4.3, the surface morphology of the different CrN coatings, obtained from SEM, is displayed. It can be clearly seen that a large quantity of both porosity and macroparticles was visible in the surface of the commercial coating than was observable in the other in-house deposited coatings.

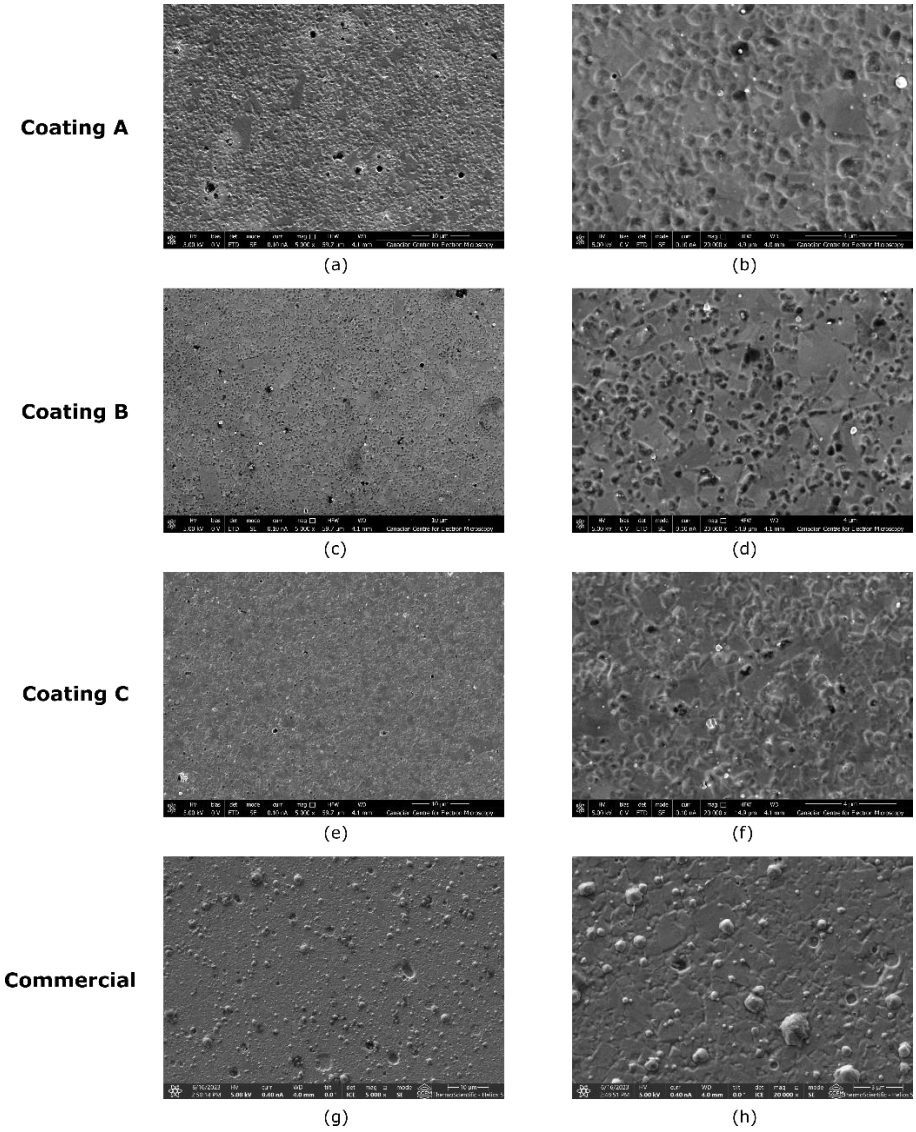

Figure 4.3 SEM images of the surface morphology of different CrN coatings: (a,c,e,g) at lower magnification; (b,d,f,h) at higher magnification

Figure 4.4 was obtained from the surface morphology of the coatings and it can be seen that with increased N_2 gas pressure, the area fraction of macroparticle density decreased, whereas no significant changes could be observed in the area fraction of porosity. However, both the area fraction of macroparticle density and the area fraction of porosity were higher for the commercial coating than for the in-

house deposited coatings. The optical representation of SEM images (Figure 4.2 (g,h)) also supports the data. The presence of macroparticle density is not only visible in the surface but also in the coating structure (Figure 4.2 (g)).

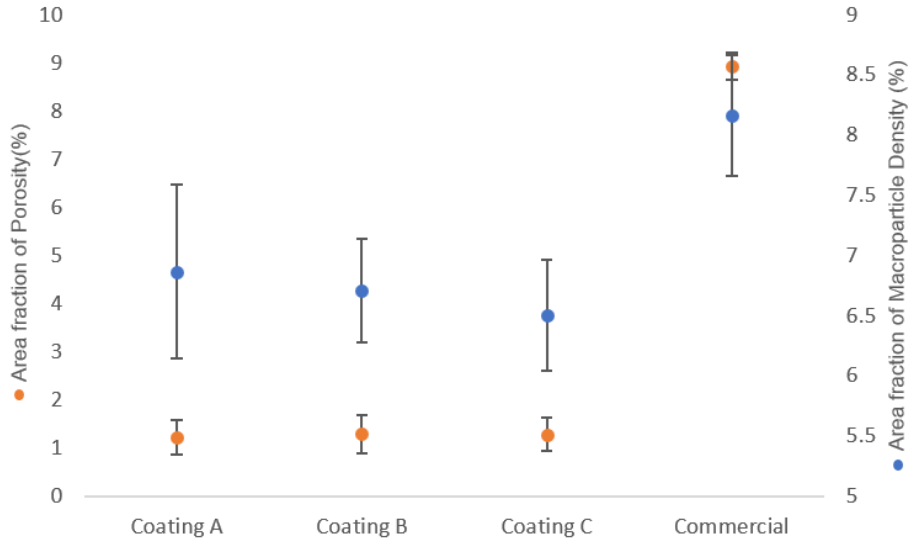

Figure 4.4 Area fraction of porosity and macroparticle density of different CrN coatings

The atomic force microscope (AFM) images of all the CrN coatings are shown in Figure 4.5. A scanning area of 2 µm x 2 µm was used for measuring surface roughness (Sa). Coating B demonstrated lower surface roughness than the other CrN coatings, whereas the commercially available coating showed the highest level of surface roughness. The surface roughness value (Sa) also supports the statement (Table 4.2). A scan size of approximately 1.6 mm x 1.6 mm was used for all the CrN coatings. It has been seen in the literature that surface roughness can greatly affect a coating's frictional properties [66], and friction plays an important role during machining applications as it influences energy

consumption, productivity, and material flow at high temperatures [67]. The frictional data in Table 4.2 corroborates this statement. Of all the coatings, Coating B demonstrated the lowest surface roughness and coefficient of friction, as indicated by the data in Table 4.2. The commercial coating exhibited the highest surface roughness and coefficient of friction.

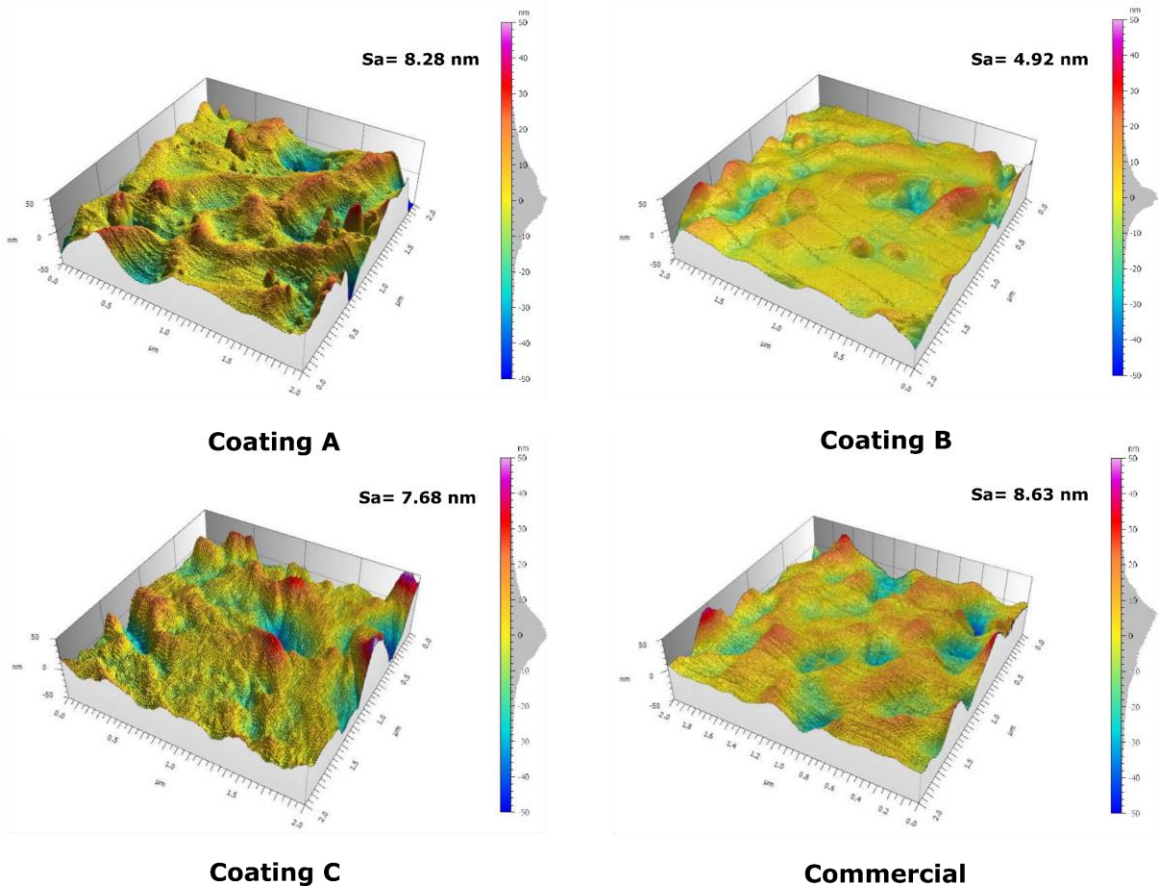

Figure 4.5 3D surface morphology of different CrN coatings with Sa values

Residual stress is an unavoidable consequence of the structural and thermal disparities between thin films and substrates. It significantly influences the properties and performance of PVD coatings, making it a crucial factor to consider.

A decrease in compressive residual stress was observed when N_2 gas pressure was higher (Table 4.2). A similar trend was reported previously by other researchers [6], [17]. This change in compressive residual stress can be attributed to a decrease in ion bombardment energy. When N_2 gas pressure is high, the likelihood of particle collision is higher, leading to less ion bombardment energy and, consequently, reducing residual stress. Although high bombardment energy can enhance atom implantation and potentially improve adhesion, excessive compressive stress can have detrimental effects on coating adherence, including coating delamination [6], [68]. From Table 4.2, it can be seen that Coating A exhibited the most compressive residual stress, and the commercial coating had the least. Neither case is viable for a coating as both can adversely affect coating adhesion and result in brittle failure. Thus, it is crucial to find balance in the coating's compressive residual stress to promote strong adhesion while ensuring desirable mechanical properties. This assertion is supported by the scratch data which is discussed in section 4.1.2.

4.1.2 Mechanical Analysis

Table 4.2 presents an overview of the micro-mechanical properties and residual stress measurements of the CrN coatings. The data in Table 4.2 clearly indicates a decreasing pattern in hardness values from Coating A to Coating C. This is due to the increase in N_2 gas pressure [6], [69]. With low N_2 gas pressure, the particles' high kinetic energy led to re-sputtering and bombardment, facilitating the formation of a compact structure, and increasing hardness [16]. All the CrN

coatings demonstrated similar hardness values with no significant differences. As illustrated in Figure 4.6, the highest elastic modulus value was observed for Coating B (Figure 4.6 (b)). Previous research has shown that coatings possessing slightly lower hardness values which also exhibit a higher elastic modulus tend to perform better [70].

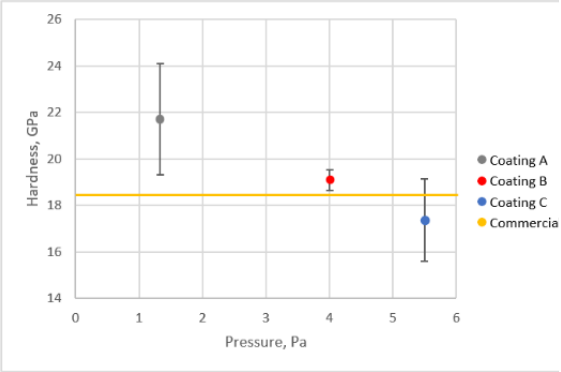

(a)

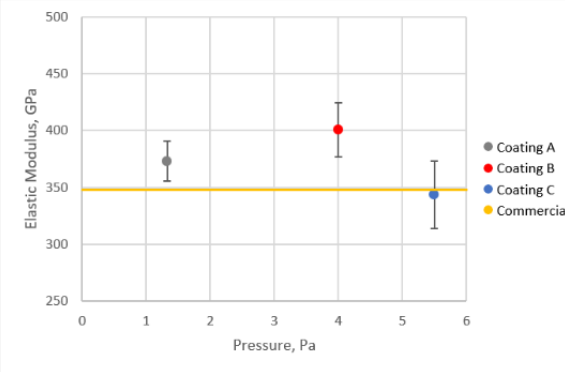

(b)

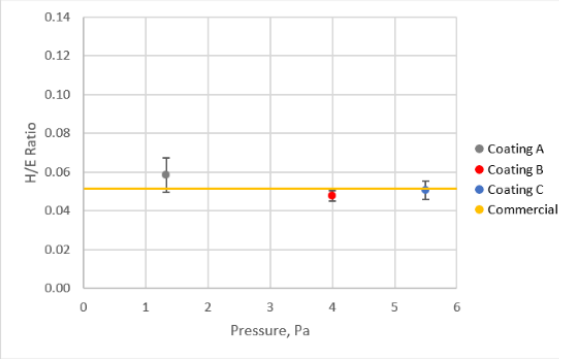

(c)

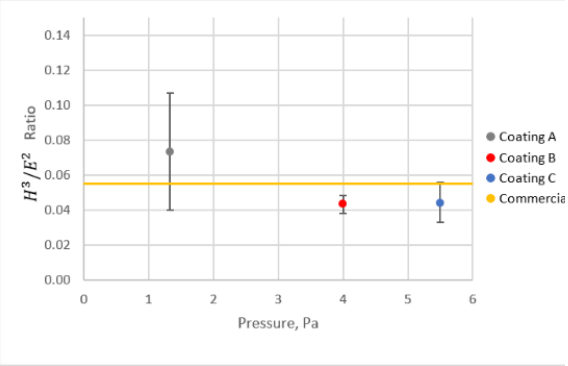

(d)

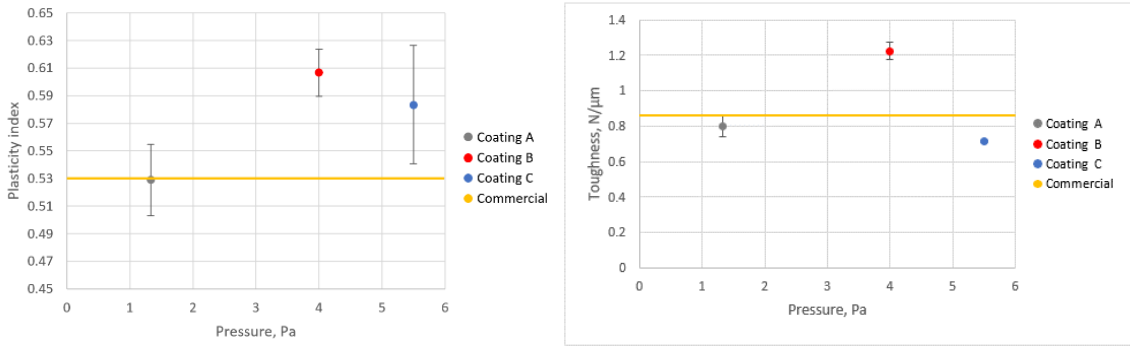

(e) (f)

Figure 4.6 Micro-mechanical properties of various CrN coating: (a) Hardness, (b) Elastic Modulus, (c) H/E ratio, (d) H^3/E^2 ratio, (e) Plasticity index and (f) Toughness

Moreover, studies have indicated that the wear resistance of such coatings improves with the increase in elastic modulus [71], [72]. A relatively high elastic modulus is advantageous as it hinders the advancement of pre-existing cracks within the material [73]. A high elastic modulus also infers that the coating is stiffer and stays elastic (retains its original shape) for a longer period of time when subjected to external forces. Although hardness is an indicator of wear resistance, H/E and H^3/E^2 ratios are also used for predicting the wear behaviour of a coating. Coatings with lower H/E and H^3/E^2 ratios have been found to perform better in adhesion dominant situations. A longer tool life has also seen for lower ratios of H/E and H^3/E^2 [1], [2]. Both H/E and H^3/E^2 ratios were lower for Coating B and higher for Coating A (Figure 4.6 (c) and Figure 4.6 (d)). These lower H/E and H^3/E^2 ratios indicate that Coating B was less brittle than the other coatings, which is further corroborated by its higher plasticity index value (Figure 4.6 (e)).

The plasticity index (PI) is another important parameter that refers to coatings ability to disperse energy. In applications where adhesion wear results in BUE formation, it is crucial for the coating to possess an enhanced ability to disperse the heat energy generated at the tool-workpiece interface. As energy is dispersed, less energy is integrated into the tool, resulting in less tool deformation and damage. The plasticity index can be exploited to evaluate a coating's energy dispersal capability by comparing the ratio of plastic work done to total work done during indentation. During the turning process, a higher PI improves cutting behaviour, particularly when adhesive wear predominates due to that property imparting the coating with a greater ability to disperse energy [70]. Thus, the higher PI value of Coating B indicates that the coating dispersed absorbed energy by means of plastic deformation instead of experiencing brittle fracture. Previous research has shown that a high PI index (as exhibited for Coating B) indicates greater toughness and durability [1]. Moreover, tougher coatings have exhibited enhanced wear-resistant properties [69] The modified Palmqvist toughness test results further confirm that Coating B exhibited greater toughness than the other CrN coatings. The variances in toughness values observed in Figure 4.6 (f) can be attributed to the applied coatings, as the substrate material was the same for all coatings. The properties presented in Table 4.2 indicate that Coating B had the lowest tendency to fracture of all the coatings, suggesting a strong resistance to brittleness. As BUE is unstable and periodically breaks off during machining, a coating with a comparatively high elastic modulus, low H/E ratio, high plasticity

index, and high toughness demonstrates superior wear performance and tool life [1]. A coating that exhibits brittle failure is more susceptible to delamination during BUE removal. Coating B's properties are therefore crucial for improving wear performance.

Figure 4.7 and Table 4.3 demonstrate the scratch behaviour of all the CrN coatings, displaying the critical loads: L_{c1}, which signifies cohesive failure or the start of initial failure, and L_{c2}, which indicates substrate exposure due to adhesive failure. The initial jump seen in the acoustic emission data in Figure 4.7 could be linked to hitting a porous structure during the scratch test. The scratch test results demonstrate somewhat similar trends for all the tested coatings. However, in the case of Coating B, while cohesive failure commenced slightly earlier than in the commercial coating, a more localized final failure suggests plastic failure as opposed to sudden brittle failure. This early cohesive failure might contribute to an overall structure that releases energy gradually. When combined with the micro-mechanical properties, these findings indicate the superior performance of Coating B. In machining processes that generate BUE, drastic failures, like the one the commercial coating had, signify a propensity for brittle failure and material removal in large quantities when the BUE breaks. From a machining perspective, this micro-mechanical property could offer distinctive advantages, specifically a resistance to chipping. Furthermore, because of this, Coating B has a lower likelihood of substrate exposure if the coating fails, indicating that this coating layer offers better surface protection than the others.

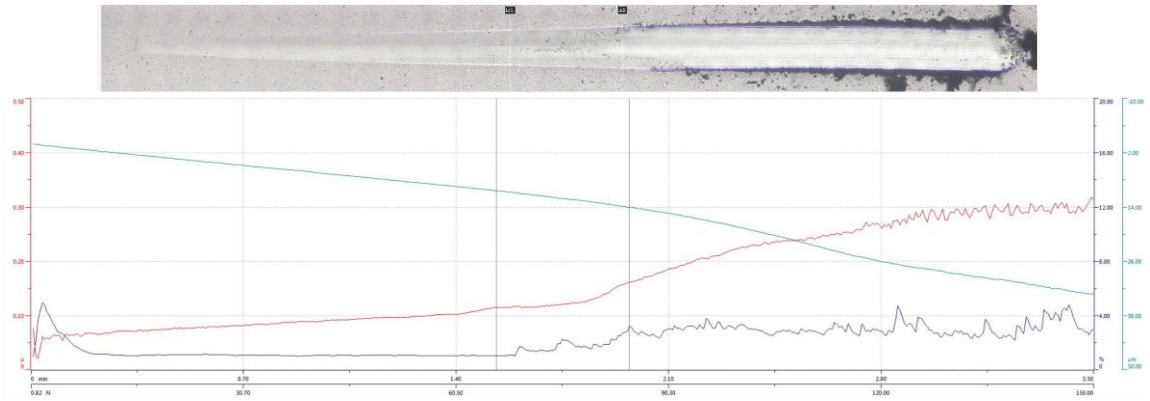

(a)

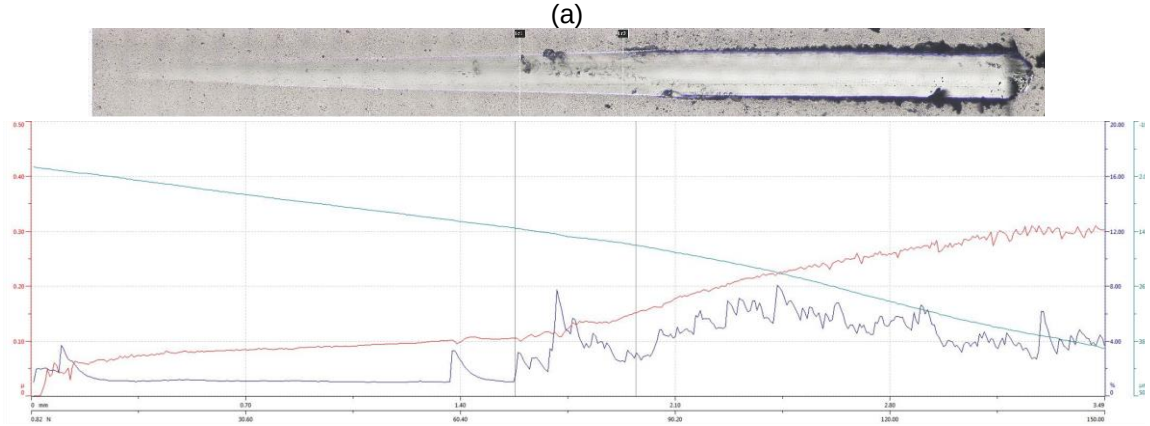

(b)

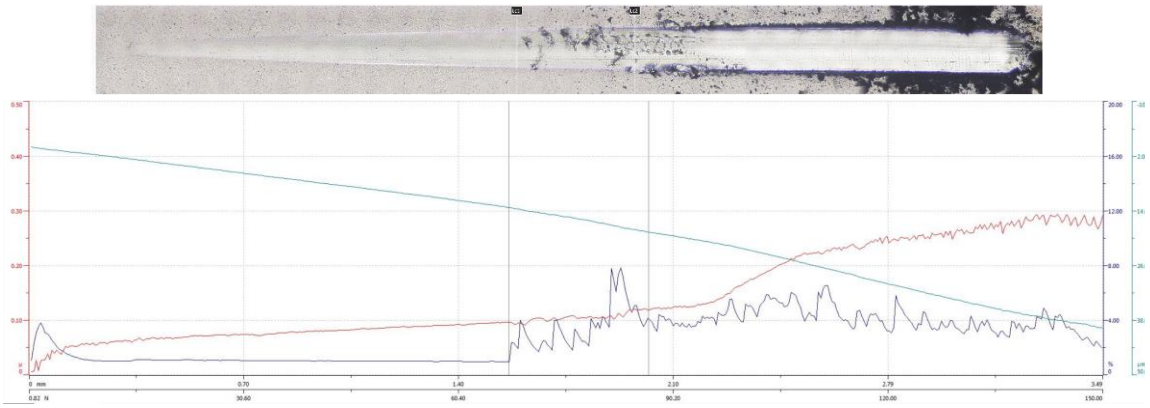

(c)

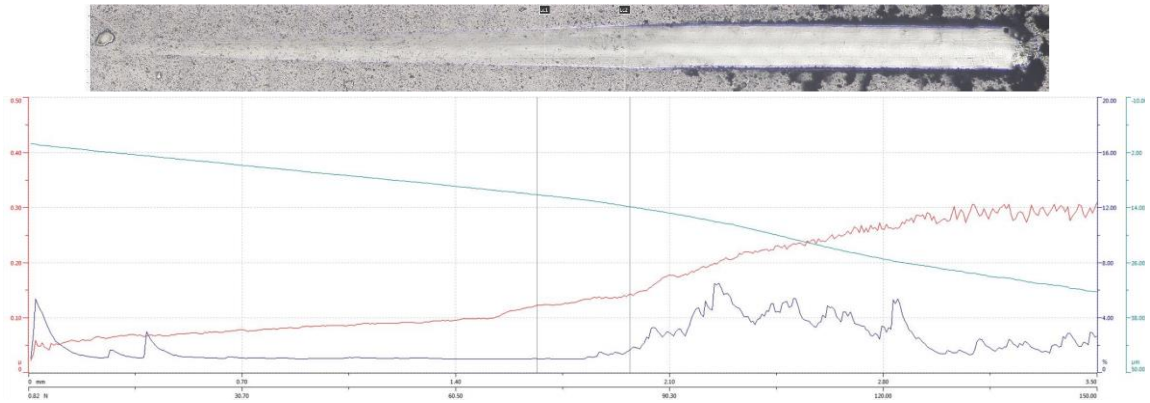

(d)

Figure 4.7 Optical representation of the scratch track with scratch test data (Green- Penetration depth, Red- Coefficient of friction and Blue- Acoustic emission) for CrN coatings: (a) Coating A, (b) Coating B, (c) Coating C, and (d) Commercial

Table 4.3 Critical load for L_{c1} (adhesive failure) and L_{c2} (cohesive failure) obtained from scratch test data for CrN coatings

Coating	L_{c1}, mm	L_{c2}, mm
Coating A	1.54	1.97
Coating B	1.56	1.97
Coating C	1.56	2.02
Commercial coating	1.67	1.97

4.1.3 Tribological Analysis

The tribological characteristics of the coatings were evaluated at an ambient temperature using a pin-on-disk tribometer in dry sliding conditions. Figure 4.8 represents the coefficient of friction data and Figure 4.9 depicts the wear track morphologies along with the width of the wear track for each CrN coating. The data clearly demonstrates that Coating B had the lowest friction coefficient value, approximately 0.15, whereas the commercial coating had the highest friction coefficient value, approximately 0.43 (Table 4.2). The high coefficient of friction value observed in the commercial coating can be attributed to the occupancy of

more macroparticle density and porosity (Figure 4.4). Its surface roughness value also corroborates this statement (Table 4.2). Conversely, Coating B exhibited enhanced frictional characteristics which can be ascribed to its smoother surface. The optical representation of the CrN coatings' wear track data, shown in Figure 4.9, further supports this finding. Of all the coatings, Coating B exhibited the least amount of wear on the track and a narrower wear track, indicating excellent frictional properties. The low coefficient of friction and the smaller wear scar area of Coating B could be related to the coating's high elastic modulus value (Table 4.2), as a coating's ability to resist wear increases as the elastic modulus increases [71], [72]. It needs to be noted that the tests were done at room temperature. The seizure effect was not considered in this study. Only sliding zone was considered. At very high temperature or high load condition seizure can happen that can affect real value of coefficient of friction.

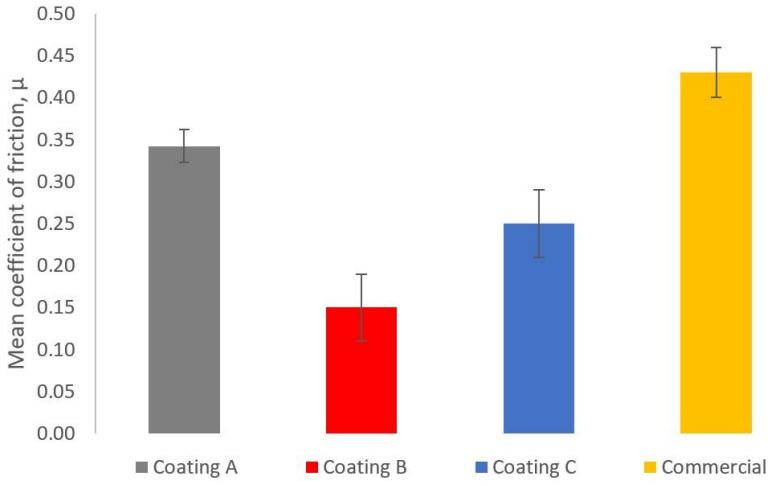

Figure 4.8 Coefficient of friction data for all the CrN coatings

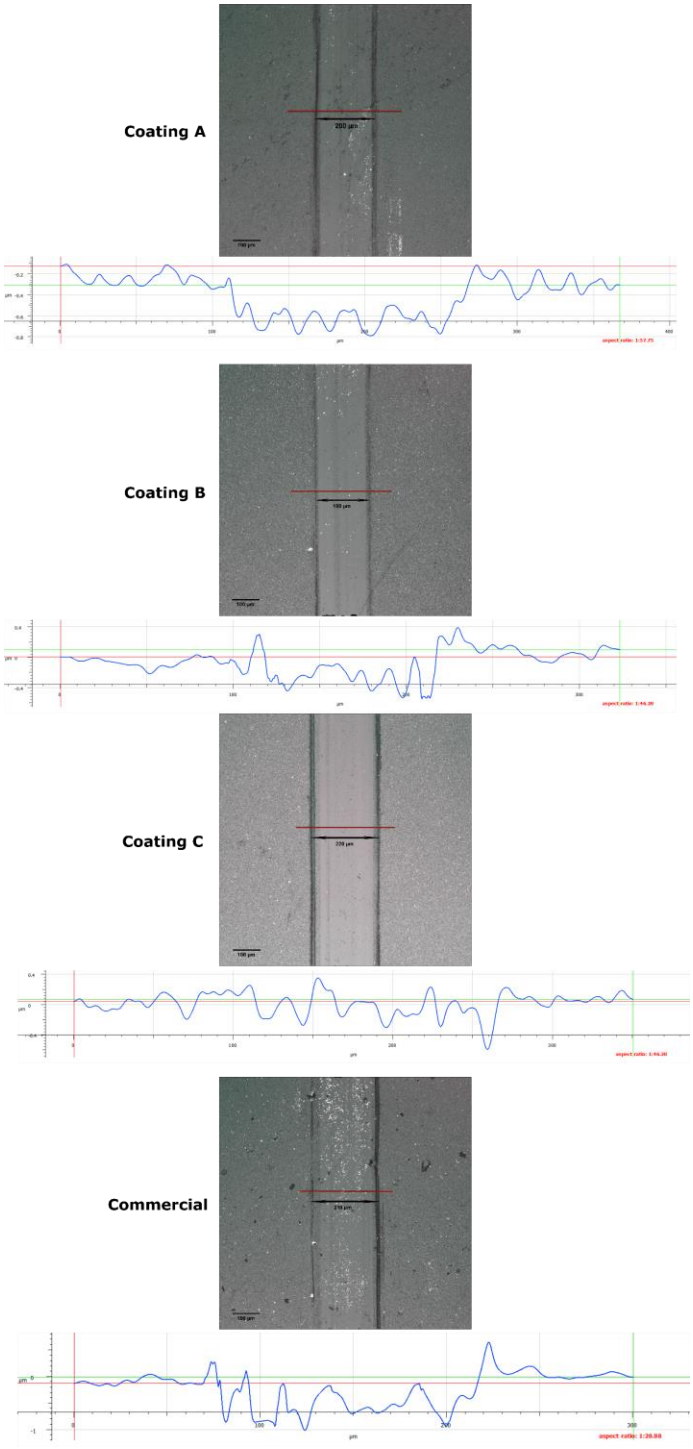

Figure 4.9 Profile Form Measurement of different CrN coatings: (a) Coating A (b) Coating B (c) Coating C, and (d) Commercial

4.2 Machining Studies

4.2.1 Tool Life Analysis

A previous demonstration revealed that coatings with a high PI coupled with a low H/E ratio exhibit enhanced tool wear performance and extended tool life during machining when adhesive-related issues are dominant [1], [2]. In the characterization studies for this thesis, a high elastic modulus, a low H/E ratio and a high PI were seen for Coating B, so Coating B was expected to exhibit less tool wear and better tool life performance than the others. To evaluate coating's performance, cutting tests and tool life studies were carried out during the dry finish turning of SS 304. A performance assessment of the tool was done by analyzing the graphical presentation of flank wear and 3D images of tool failure, as shown in Figures 4.10 and 4.11. Among all the coatings, the best-performing CrN-coated tool was Coating B, which also means that Coating B exhibited the lowest wear rate in comparison to the other CrN-coated tools. Coating A showed the most intense flank wear followed, in order from most to least, by the uncoated tool, Coating C, the commercial coating, and Coating B. Coating B had an approximately 19% improvement in tool life compared to the uncoated tool and approximately 8% compared to the commercial coating.

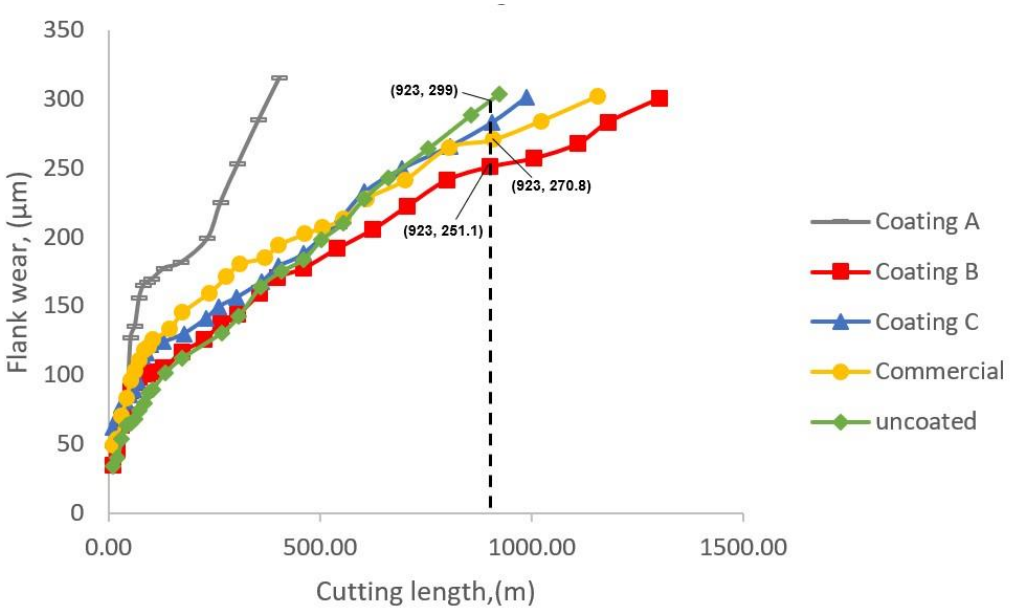

Figure 4.10 Cutting test results: Tool flank wear progression vs. cutting length

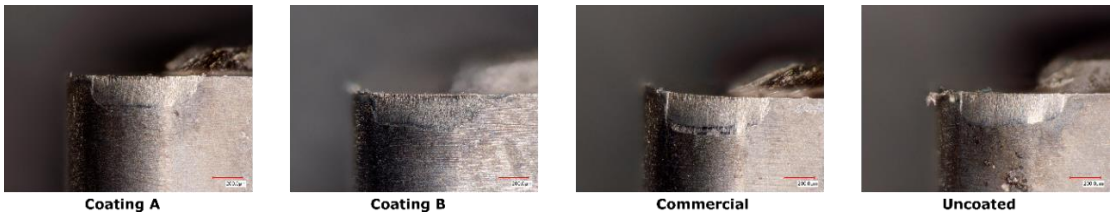

Figure 4.11 3D tool wear images of tools at a cutting length of approximately 600 m during the dry finish turning of AISI 304

A succession of progressive wear tests were carried out to examine the superior performance of Coating B and to learn more about the mechanism of tool wear. After every 200 meters of cutting length, the tool's wear patterns were examined along with 3D optical imaging to add more visual information. As can be seen from Figure 4.12, two wear mechanisms were responsible for the majority of tool wear which mainly happened near the cutting edge. The first mechanism involved the adhesion of the work piece material, which formed a built-up edge at the cutting edge of the tool, whereas the second mechanism, crater wear, was

caused due to elevated cutting temperatures. The progression of BUE formation (any peaks above the original tool's reference surface) and crater wear (any peaks below the original tool's reference surface) for all the cutting inserts are demonstrated in Figures 4.13 and 4.14. It has already been mentioned that having a property combination like Coating B's is crucial in environments where adhesion wear results in BUE formation. Figures 4.13 and 4.14 reinforce that statement. The least overall BUE formation was also observed for Coating B. At 400 m of cutting length, however, Coating B showed a slight up-tick in BUE (Figure 4.13) and a sharp drop in crater wear (Figure 4.14) because the crater wear was filled in by BUE material. Past 400 m of cutting length, Coating B maintained the least BUE formation among all the cutting tools. Coating B displayed little tendency towards BUE generation and a low gradual build-up during cutting, results which indicate a lower tendency of edge chipping. Therefore, lower BUE generation, coupled with delayed and reduced progressive crater wear, provided a more consistent and stable pattern of tool wear for Coating B (Figure 4.13-4.14). A 3D representation of tool wear on all the coated and un-coated tools at approximately 600 m of cutting length also showed comparatively less BUE formation on Coating B than on the others (Figure 4.11). However, the crater volume was the lowest for uncoated tools compared to other coatings because of the intensive BUE concealing the crater wear on the tool's rake surface (Figure 4.12-4.14). Figure 4.15 represents the force component measurements for all the CrN coated and uncoated tools. From the force data, it can be seen that Coating B generated lower forces than the other

coatings. It is important to note that the BUE formation aligns with the force measurements. The similarity in the cutting-edge radius of each coated tool, as shown in Table 4.2, demonstrates that the differences in the force data were caused solely by variations in the coatings and not by any changes in the tool's micro-geometry.

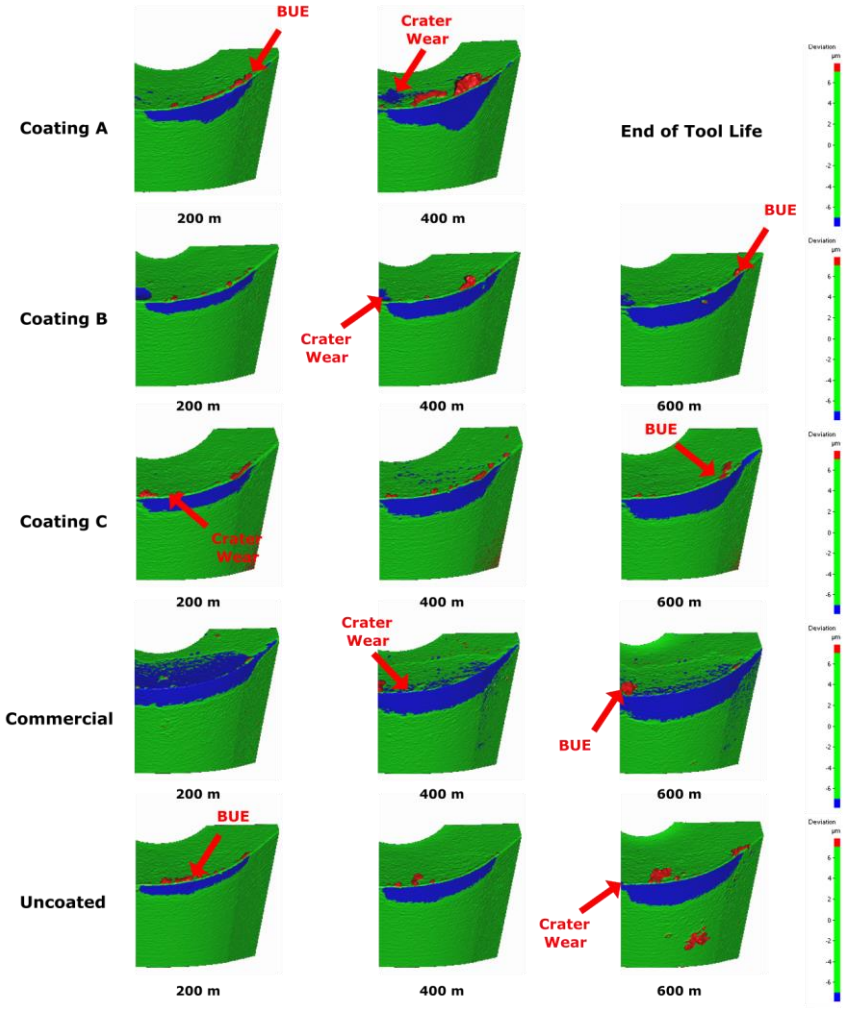

Figure 4.12 Development of tool wear (BUE and crater wear) after every 200 m length for all the CrN coated and uncoated tools: (a) 200 m, (b) 400 m, and (c) 600 m

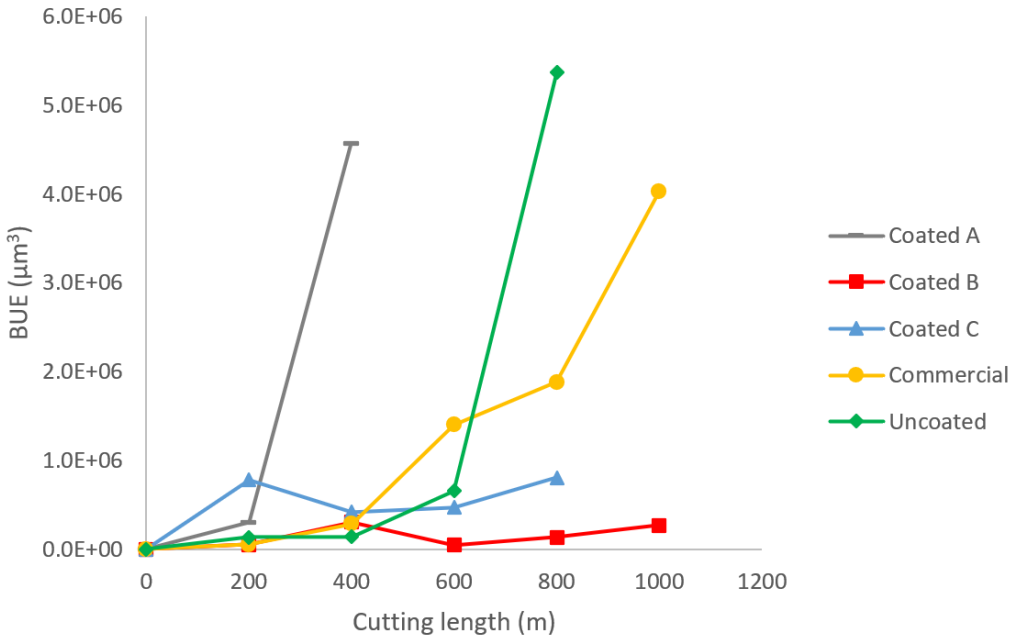

Figure 4.13 Volumetric progression of BUE for CrN coated and uncoated tools with respect to cutting length

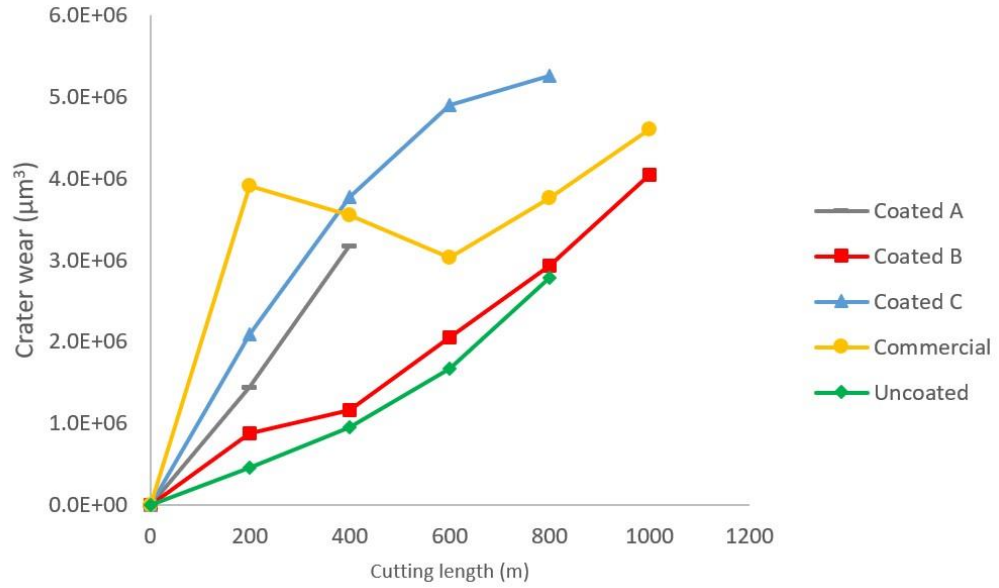

Figure 4.14 Volumetric progression of Crater wear for CrN coated and uncoated tools with respect to cutting length

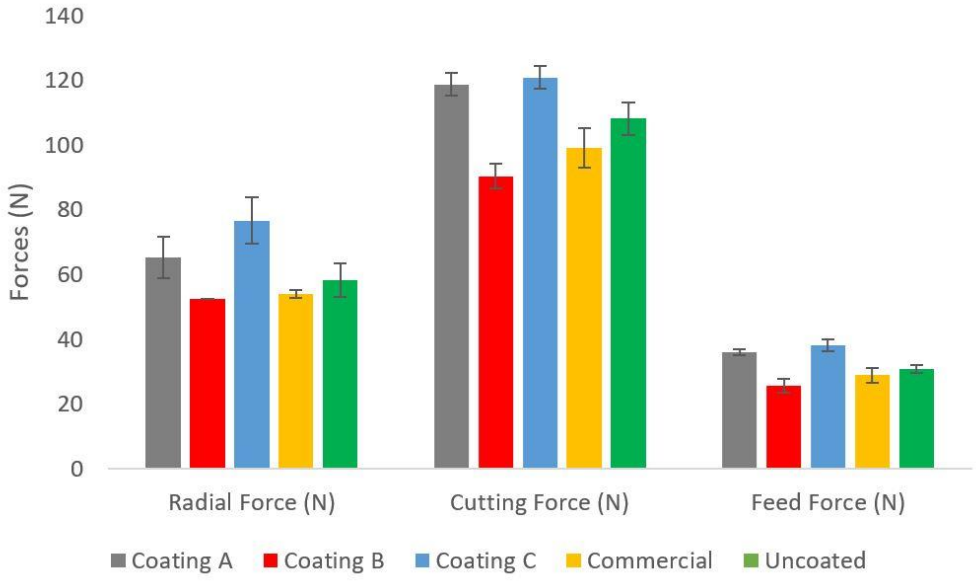

Figure 4.15 Cutting force data for all the coated and uncoated tools

4.2.2 Evaluation of Tribological Performance

From Figure 4.12, it is apparent that Coating B performed the best in reducing BUE formation compared to the other coated and uncoated tools. This is due to its micro-mechanical properties such as its high elastic modulus, low H/E ratio, and high plasticity index (Table 4.2). Aside from micro-mechanical properties, the tribological properties of a coating is also influential in reducing BUE formation and improving tool life. To acquire insights into the influence of the entire substrate/coating system on chip formation, in-situ tribological assessments were conducted which analyzed chip characteristics. Table 4.4 summarizes the attributes of the chips gathered after roughly 10 m of cutting length. The analysis of the chip characteristics revealed that Coating B's tribological behaviour was more favourable than the other coated and uncoated tools. Both the CCR and SA were higher for Coating B, indicating low cutting and frictional forces at the interface

of the tool-chip because of weaker shearing forces. This observation is consistent with the cutting force data (Figure 4.15).

Table 4.4 Chip characteristic studies for evaluating tribological performance

Tools	Chip Compression Ratio-CCR	Shear Angle, Φ (˚)	Chip Sliding Velocity (m/min)	Chip Undersurface Roughness, S_a (µm)
Coating A	0.66	36.28	79.19	1.48±0.1
Coating B	0.87	45.26	104.39	0.79±0.03
Coating C	0.63	34.86	75.59	1.16±0.18
Commercial	0.77	41.19	92.38	1±0.04
Uncoated	0.68	37.2	81.57	1.23±0.1

Furthermore, the chip sliding velocity was higher for Coating B, confirming that the flow was accelerated in the cutting zone with less friction present at the tool-chip interface as well as a shorter tool-chip contact length. This complements the coefficient of friction data (Figure 4.16).

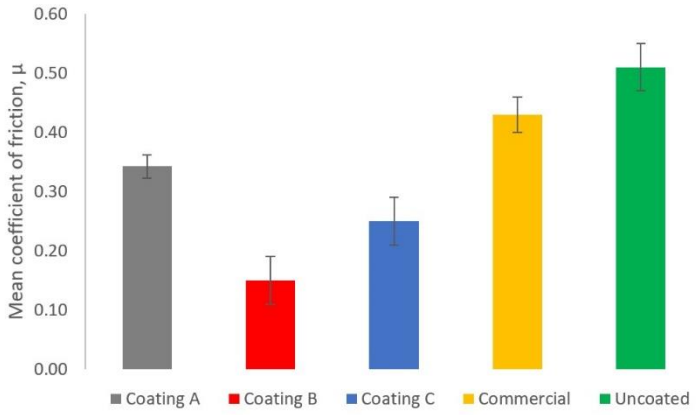

Figure 4.16 Coefficient of friction data for all the coated and uncoated tools

The surface topography of chip undersurfaces was investigated to validate the hypothesis that Coating B's coating-substrate interface generates increased flow of the chip at the tool/chip interface. The chip produced by Coating B had a smoother surface contrasted to the other coated and uncoated tools (Figure 4.17). These results further confirm that the coating/substrate system of Coating B had superior characteristics. Therefore, it can be inferred that Coating B's integrative coating/substrate system was ideal for reducing BUE formation, resulting in an overall enhancement in tool life.

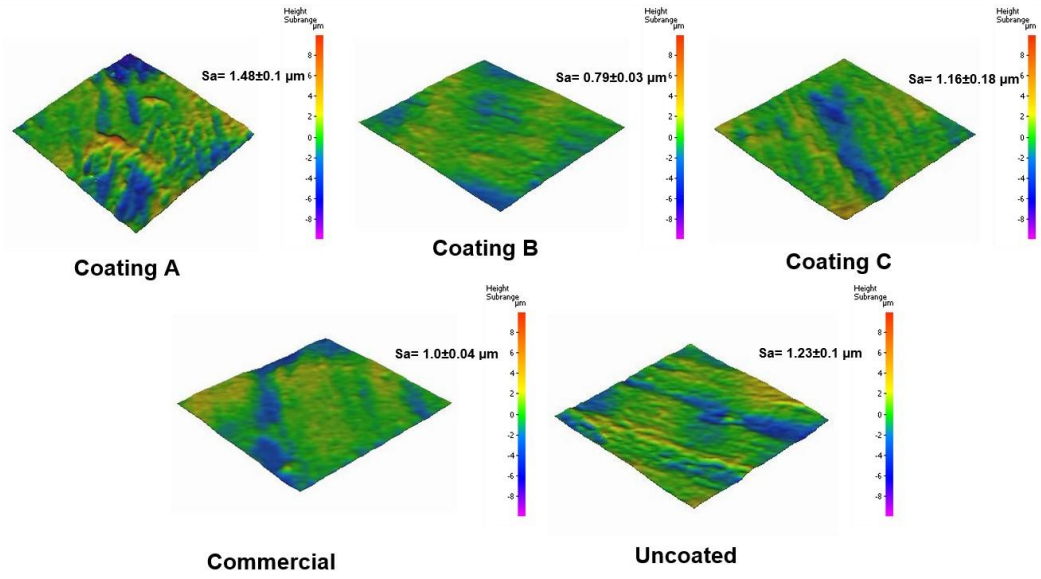

Figure 4.17 3D surface texturing of all the chips' undersurfaces

4.3 High-Temperature Studies

In previous machining studies Coating B showed improved tool performance and prolonged tool life in environments where adhesion wear results in BUE formation [1], [74]. The micro-mechanical properties of Coating B were thoroughly investigated at room temperature to understand its better performance. Coating B showed the best property-performance relationship compared to any other coatings developed in-house as well as the commercial coating. A follow-up investigation was done to investigate the effects of high temperatures (up to 450 ˚C) on Coating B's structural, mechanical, and tribological properties and compare its high-temperature properties with the commercial coating.

Figure 4.18 shows the SEM images of Coating B and the commercial coating at 150 ˚C, 250 ˚C, 350 ˚C, and 450 ˚C. It can be clearly seen in the figure that the increase in temperature resulted in hardly any change in Coating B's surface, whereas the porosity and macroparticle density became more visible on the surface of the commercial coating. It has been mentioned previously that both porosity and macroparticle density can have a detrimental effect on a coating's micro-mechanical properties, performance, and topography [64], [65]. This aligns with the micro-mechanical properties (Figure 4.19) and surface topography (Figure 4.20) findings.

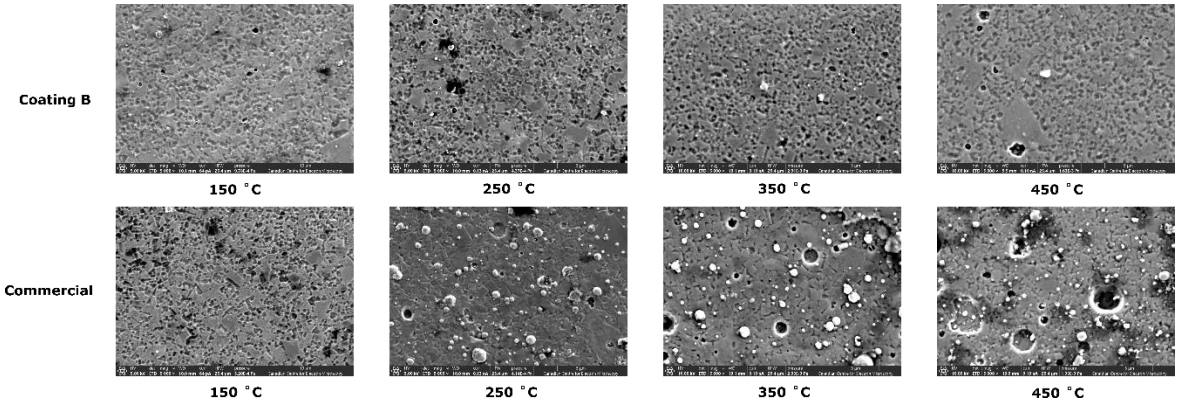

Figure 4.18 SEM images of the surfaces of Coating B and the commercial coating at 150 ˚C, 250 ˚C, 350 ˚C and 450 ˚C temperatures

Figure 4.19 shows the surface topography of Coating B and the commercial coating at different temperatures. A scanning area of 2 μm x 2 μm was used to measure the arithmetic mean height (Sa) values. Coating B showed a lower surface roughness value than the commercial coating at different temperatures. Although both coatings exhibited an increase in surface roughness values as the temperature rose, the commercial coating had a more pronounced increase in surface roughness values than Coating B. The increase in the surface roughness values from 7.68 nm at 150 ˚C to 21.4 nm at 250 ˚C was due to the prominence of porosity and macroparticle density as both became more visible on the surface of the commercial coating starting at 250 ˚C (Figure 4.19). The measured surface roughness value also confirmed this (Figure 4.20 (g)). From Figures 4.20 (a) and 4.20 (b), it can be clearly seen that temperature affected both the hardness and elastic modulus less for Coating B than it did for the commercial coating, meaning that Coating B maintained its hardness values without compromising its elastic modulus values. Coating B had an approximately 3.6% reduction in hardness and

a 13.8% increase in elastic modulus throughout the rise in temperature from room temperature to 450 ˚C. The hardness and elastic modulus values of the commercial coating, however, decreased by approximately 67.4% and 23.3%, respectively. It can therefore be concluded that the properties of the commercial coating deteriorate more at higher temperatures whereas Coating B is less affected by temperature.

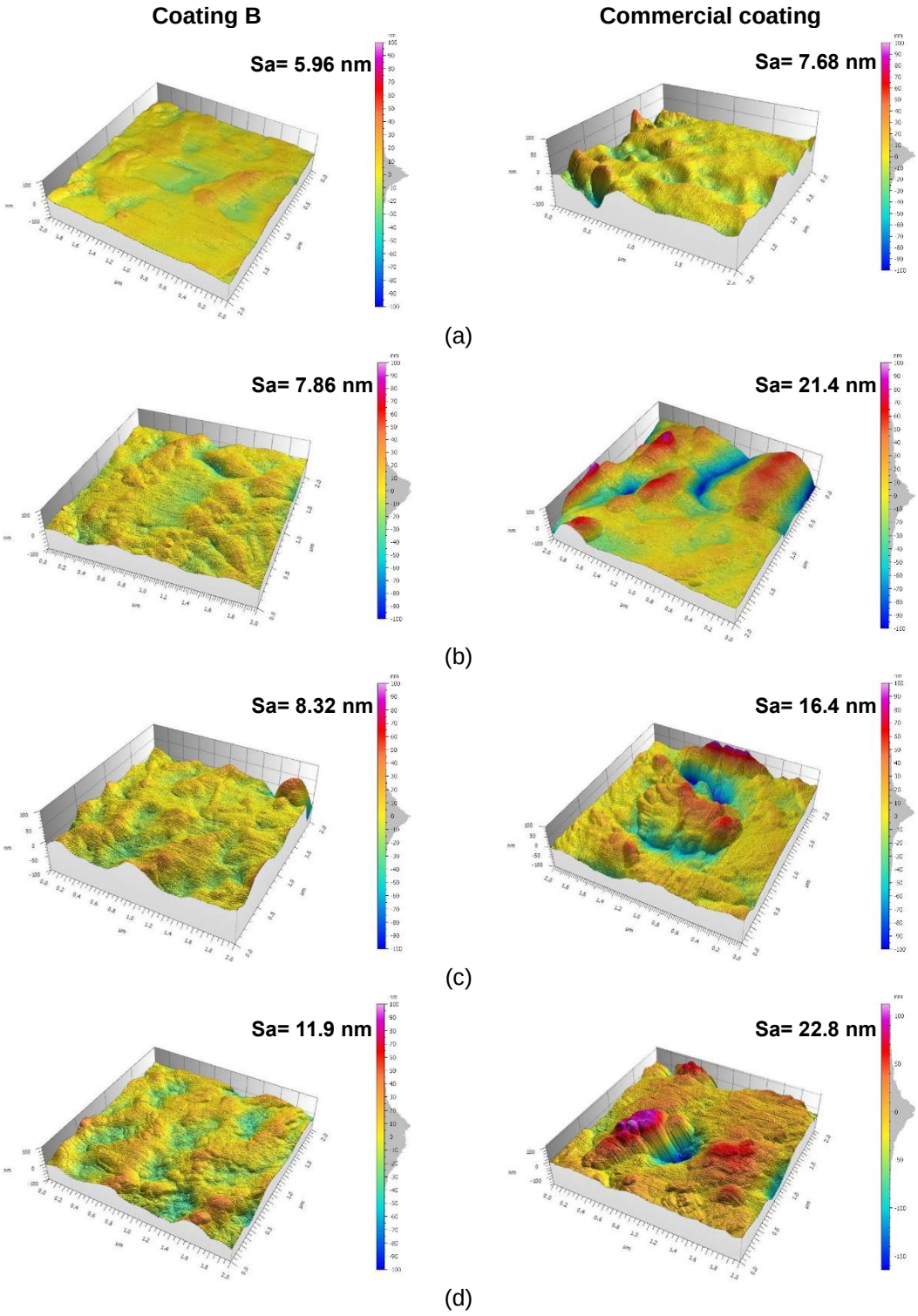
Coating B
Commercial coating
Sa= 5.96 nm
Sa= 7.68 nm
(a)
Sa= 7.86 nm
Sa= 21.4 nm
(b)
Sa= 8.32 nm
Sa= 16.4 nm
(c)
Sa= 11.9 nm
Sa= 22.8 nm
(d)

Figure 4.19 3D surface morphology of Coating B and the commercial coating with Sa values at different temperatures: (a)150 ˚C, (b) 250 ˚C, (c) 350 ˚C, and (d) 450 ˚C

It has been previously mentioned that a low H/E ratio, a low H^3/E^2 ratio, and a high plasticity index are beneficial for machining sticky materials and reducing BUE formation [64], [65]. The commercial coating demonstrated a low H/E ratio (Figure 4.20 (c)), a low H^3/E^2 ratio (Figure 4.20 (d)), and a high plasticity index (Figure 4.20 (e)) with the increase in temperature, but it achieved those properties by compromising its elastic modulus. A previous investigation showed that a substantial mismatch between the elastic modulus values of the coating and substrate can induce unwanted stress and affect the coating's wear performance [75]. Conversely, without compromising the elastic modulus, Coating B showed an approximately 16.7% decrease in its H/E ratio, 30.2% decrease in its H^3/E^2 ratio, and 13.8% increase in its plasticity index as it heated from room temperature to 450 ˚C. This, too, indicates that Coating B is more likely to fail from plastic deformation than brittle failure. Coating B also showed a more favourable toughness value than the commercial coating throughout the temperature increase. Properties suited to high temperatures, like Coating B's, are beneficial in heavy-load machining applications with BUE generation because of their superior ability to resist wear and reduce BUE.

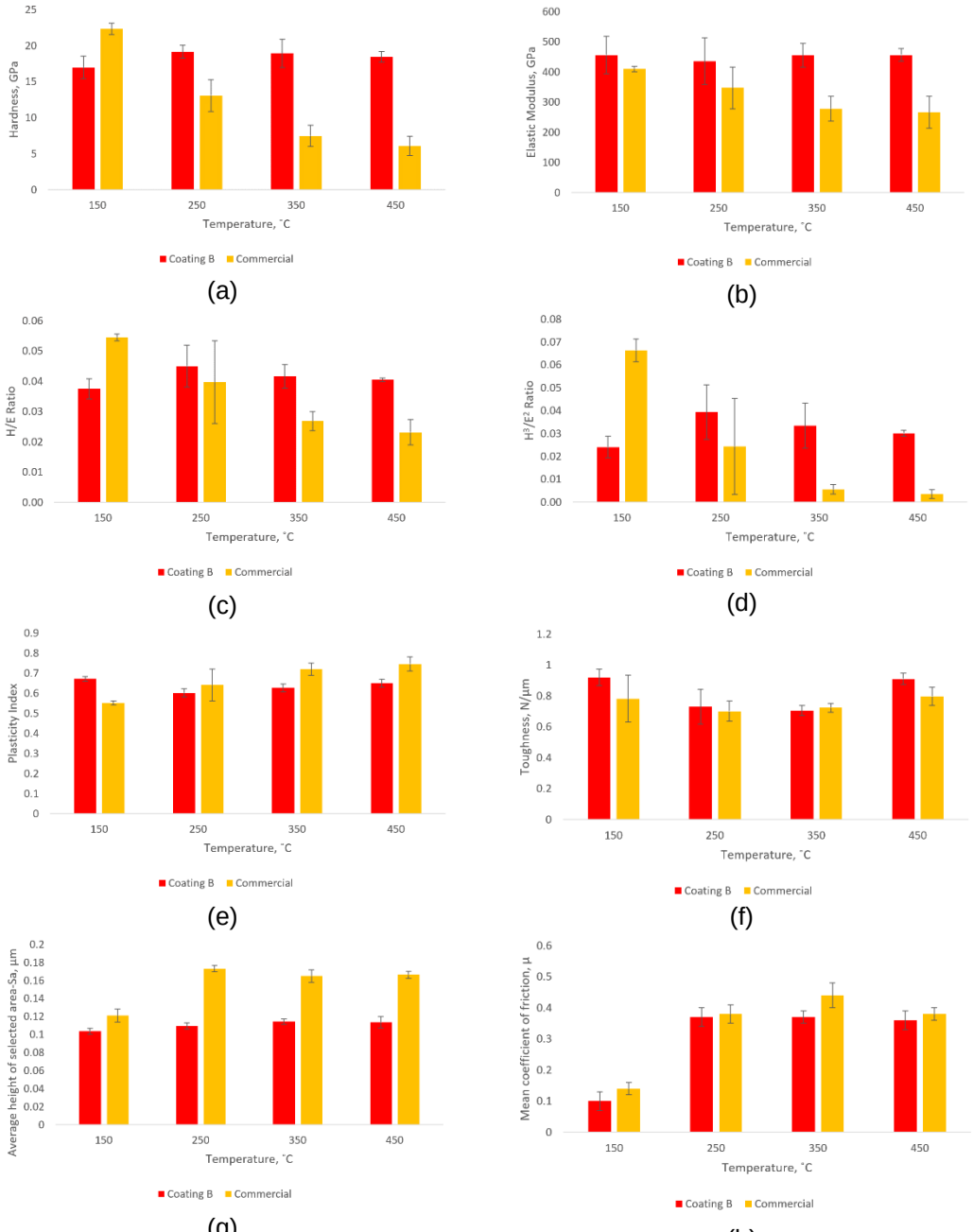

Figure 4.20 Micro-mechanical properties of Coating B (Red) and the commercial coating (Orange) at different temperatures: (a) Hardness, (b) Elastic Modulus, (c) H/E ratio, (d) H^3/E^2 ratio, (e) Plasticity index, (f) Toughness, (g) Average height of selected area (S_a) and (h) Mean coefficient of friction

Figure 4.21 and Table 4.5 show the room temperature scratch test results and the critical loads L_{c1} (crack initiation or cohesive failure) and L_{c2} (coating failure

or adhesive failure) for Coating B and the commercial coating which were heated up to 450 ˚C. The bumps that can be seen in the acoustic emission data (depicted in blue) can be attributed to impacts on porosity. As the temperature rose from room temperature to 450 ˚C, adhesive failure (L_{c1}) started earlier for Coating B than for the commercial coating (Figure 4.21). Cohesive failure (L_{c2}) for both coatings started at a similar point from room temperature, but as the temperature reached 450 ˚C, the commercial coating exhibited a decrease of approximately 10.2% in L_{c2} while Coating B, approximately 7.6% (Table 4.5). This scratch test data indicates, just like the micro-mechanical property data, that Coating B is better in retaining its original properties than the commercial coating at high temperatures.

Table 4.5 Critical load for L_{c1} (adhesive failure) and L_{c2} (cohesive failure) obtained from scratch test data for Coating B and the commercial coating.

Temperature	Coating B		Commercial coating	
	L_{c1}, mm	L_{c2}, mm	L_{c1}, mm	L_{c2}, mm
Room temperature	1.56	1.97	1.67	1.97
150 ˚C	1.6	1.89	1.55	1.87
250 ˚C	1.36	1.93	1.63	1.99
350 ˚C	1.42	1.8	1.54	1.86
450 ˚C	1.29	1.82	1.46	1.77

Coating B **Commercial coating**

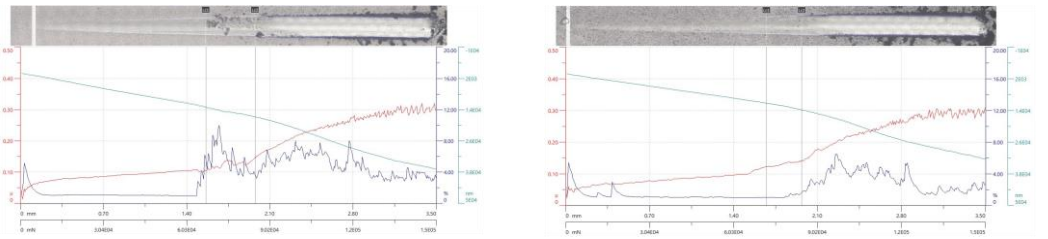

(a)

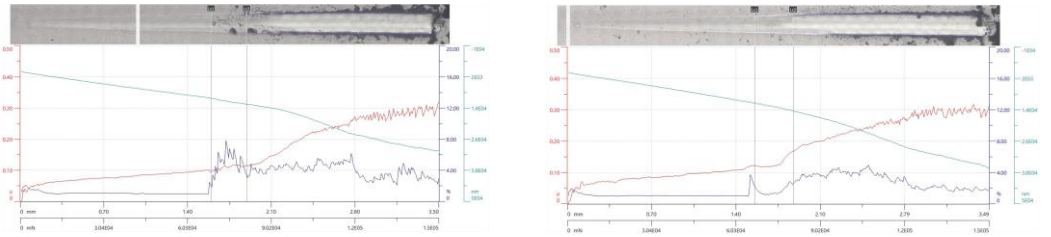

(b)

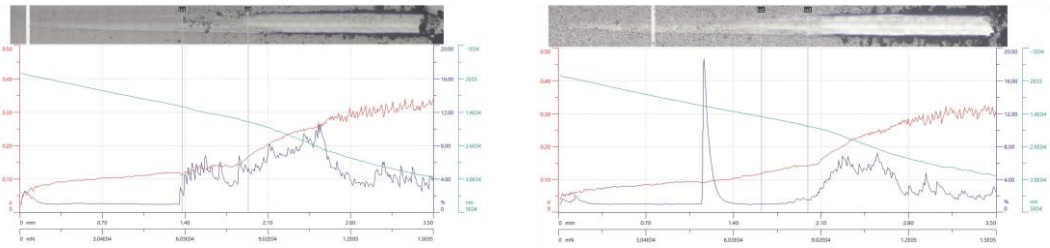

(c)

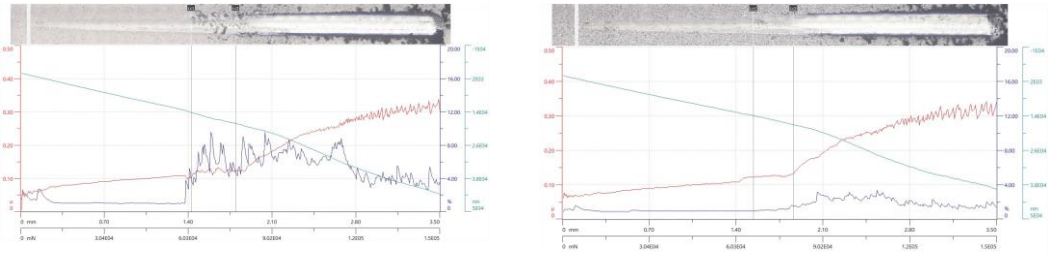

(d)

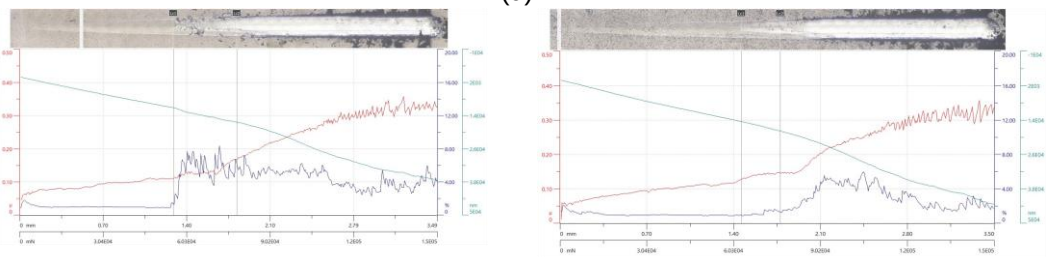

(e)

Figure 4.21 Optical representation of the scratch track with scratch test data (Green- Penetration depth, Red- Coefficient of friction and Blue- Acoustic emission) for Coating B and the commercial coating: (a) RT, (b)150 ˚C, (c) 250 ˚C (d) 350 ˚C, and (e) 450 ˚C

The coefficient of friction data obtained from the scratch test data also shows that Coating B had a more favourable frictional value. Throughout the increase in temperature from room temperature to 450 ˚C, Coating B experienced an approximately 6.4% increase in the coefficient of friction, whereas the commercial coating had about a 9.5% increase. The SEM images (Figure 4.18) offer a probable reason for the difference: at 450 ˚C, the surface of the commercial coating had more porosity and macroparticle density than Coating B did, making it less resistant to oxidation. Therefore, in machining applications with BUE formation, the commercial coating is likely to delaminate by drastic failure and experience poor tool performance at high temperatures. For high-temperature machining applications with adhesive wear that results in BUE formation, Coating B is a more viable solution because of its excellent high-temperature properties (Figure 4.20) along with its gradual plastic deformation and better coefficient of friction (Figure 4.21).

Chapter 5 – CONCLUSION AND FUTURE WORKS

5.1 Conclusion

Nowadays, many machining applications where adhesion-related issues are prevalent, use self-adaptive PVD coatings. These coatings perform best when machining materials like titanium and stainless steel, as well as during stamping operations. One of the main downsides for machining these types of materials is the work material's propensity to adhere to the tool body. Such strong adhesion causes the development of BUE, an unstable structure which can carry away a significant amount of tool material when it breaks away from the tool. In order to improve overall tool performance and obtain a smoother surface finish, it is essential to reduce BUE formation. Among the self-adaptive PVD coatings, CrN coatings have gained popularity because of their excellent oxidation resistance, chemical stability, and advantageous tribological properties, as these properties play an important role in machining sticky materials.

The aim of this study was to examine the micro-mechanical properties of CrN coatings and their influence on reducing BUE formation, by adjusting N_2 gas pressure. It was determined that changing the N_2 gas pressure affects the hardness and residual stress of the coatings; a decreasing trend in these properties was observed across all the coatings, corresponding to increases in N_2 gas pressure. After an in-depth analysis, it was found that a combination of 4 Pa nitrogen gas pressure, -50 V bias voltage, and a coating thickness of 1.84±0.1 yields enhanced

micro-mechanical and tribological properties, thereby aiding in the machining process for operations dominated by BUE generation.

A thorough investigation of the micro-mechanical properties revealed that a CrN coating with a relatively high elastic modulus (E), low H/E ratio, low roughness, high toughness, and high plasticity index (PI) outperforms other tested CrN coatings, exhibiting enhanced resistance to coating delamination. Furthermore, the influence of compressive residual stress on the coating's failure behavior was significant. An optimized compressive residual stress was found to promote better adhesion in CrN coatings, enhancing their performance.

Machining studies also revealed that the above-mentioned properties in a CrN coating are beneficial for reducing adhesion wear in applications prone to BUE generation. The CrN coating deposited at 4 Pa nitrogen gas pressure and -50 V bias voltage (the best-performing coating) had a longer tool life than the other coatings. The best-performing coating showed the lowest flank wear and built-up volume progression than the other coatings. Low BUE formation in best-performing coating also demonstrates low tendency for edge chipping. This inference is supported by data showing that the tool coated using these parameters had fewer cutting forces acting against it and produced chips with relatively smooth undersurfaces.

The high-temperature study results further confirmed that compared to the tested commercial coating, the best-performing coating (deposited at 4 Pa N_2 gas

pressure, -50 V Bias voltage) displayed superior mechanical and tribological properties suitable for such applications. The best-performing coating maintained its hardness without compromising its elastic modulus. Conversely, the commercial coating experienced a significant decrease in both hardness and elastic modulus values. The commercial coating also exhibited a higher number of porosities and greater macroparticle density. Furthermore, surface roughness values and the coefficient of friction were also elevated for the commercial coating as contested to the best-performing coating.

The investigation showed that in high-temperature applications, like stainless steel machining, the commercial coating is prone to failure and poor tool performance, whereas the best-performing in-house coating, characterized by lower porosity, sparser macroparticle density, less surface roughness, and a lower coefficient of friction, demonstrates greater resilience. Coatings with these properties are likely to perform exceptionally well in high-temperature applications where the wear mechanism is influenced by BUE formation.

5.2 Recommendations for Future Works

The present research demonstrates that developing PVD coatings with a combination of properties which particularly address adhesion wear with BUE formation can improve tool life. Similar concepts and coatings can be applied to other operations for example milling, drilling, where tool performance is dictated by

adhesion wear with BUE formation. The abovementioned applications should be investigated to fully comprehend the potential of the coating.

As the focus of this study was on the development of coating, the influence of the developed coating on the machined surface was not thoroughly investigated. Therefore, to acquire a greater understanding of how the developed coating affects the workpiece, it is essential to perform surface integrity studies.

The tool's microgeometry and substrate properties can be significantly affected by the cutting-edge preparation. Cutting-edge preparation can help to minimize manufacturing defects while improving the coating's adherence and quality. To further improve the coating's quality and performance, edge preparation might be performed after the coating deposition. A thorough investigation of how various edge preparation methods affect tool performance and coating quality is necessary.

Finally, this study has introduced a solid foundation for understanding coating behaviour at high temperatures and provided a preliminary base for conducting additional high-temperature studies, including temperatures exceeding 450°C. High temperature could lead to some phase transformation. Phase transformation was not studied in this study. Phase transformation can affect coating's structure making it a crucial factor to consider in future studies.

References

[1] M. S. I. Chowdhury, B. Bose, S. Rawal, G. S. Fox-Rabinovich, and S. C. Veldhuis, “Investigation of the Wear Behavior of PVD Coated Carbide Tools during Ti6Al4V Machining with Intensive Built Up Edge Formation,” *Coatings 2021, Vol. 11, Page 266*, vol. 11, no. 3, p. 266, Feb. 2021, doi: 10.3390/COATINGS11030266.

[2] M. S. I. Chowdhury *et al.*, “Wear performance investigation of PVD coated and uncoated carbide tools during high-speed machining of TiAl6V4 aerospace alloy,” *Wear*, vol. 446–447, p. 203168, Apr. 2020, doi: 10.1016/J.WEAR.2019.203168.

[3] “Fundamentals of Modern Manufacturing Materials Processes and Systems 4th Edition”.

[4] C. M. Fernandes and A. M. R. Senos, “Cemented carbide phase diagrams: A review,” *Int J Refract Metals Hard Mater*, vol. 29, no. 4, pp. 405–418, Jul. 2011, doi: 10.1016/J.IJRMHM.2011.02.004.

[5] D. Jianxin, Z. Jiantou, Z. Hui, and Y. Pei, “Wear mechanisms of cemented carbide tools in dry cutting of precipitation hardening semi-austenitic stainless steels,” *Wear*, vol. 270, no. 7–8, pp. 520–527, Mar. 2011, doi: 10.1016/J.WEAR.2011.01.006.

[6] M. Abdoos, S. Rawal, A. F. M. Arif, and S. C. Veldhuis, “A strategy to improve tool life by controlling cohesive failure in thick TiAlN coating during turning of CGI,” *International Journal of Advanced Manufacturing Technology*, vol. 106, no. 7–8, pp. 2793–2803, Feb. 2020, doi: 10.1007/s00170-019-04854-0.

[7] K. S. Kim, H. K. Kim, J. H. La, K. B. Kim, and S. Y. Lee, “Influence of N 2 Partial Pressure on the Microstructure, Hardness, and Thermal Stability of CrZrSiN Nanocomposite Coatings 1,” *Journal of Superhard Materials*, vol. 38, no. 4, pp. 255–262, 2016, doi: 10.3103/S1063457616040067.

[8] S. Larpkiattaworn, S. Surinphong, N. Thailand, C. Busabok, and P. Termsuksawad, “Effect of Nitrogen Partial Pressure on Characteristic and Mechanical Properties of Hard Coating TiAlN Film,” 2011. [Online]. Available: https://www.researchgate.net/publication/271839341

[9] M. L. Cedeño-Venté *et al.*, “Effect of Graded Bias Voltage on the Microstructure of arc-PVD CrN Films and its Response in Electrochemical & Mechanical Behavior.”

[10] O. Lupicka and B. Warcholinski, “The Adhesion of CrN Thin Films Deposited on Modified 42CrMo4 Steel,” *Advances in Materials Science and Engineering*, vol. 2017, 2017, doi: 10.1155/2017/4064208.

[11] V. Merie, G. Negrea, M. Pustan, C. Bîrleanu, and B. Neamțu, “TRIBOMECHANICAL CHARACTERISTICS OF CHROMIUM NITRIDE THIN FILMS DEPOSITED AT DIFFERENT PARAMETERS.”

[12] H. Elmkhah, T. F. Zhang, A. Abdollah-zadeh, K. H. Kim, and F. Mahboubi, “Surface characteristics for the Ti[Formula presented]Al[Formula presented]N coatings deposited by high power impulse magnetron sputtering technique at the different bias voltages,” *J Alloys Compd*, vol. 688, pp. 820–827, 2016, doi: 10.1016/J.JALLCOM.2016.07.013.

[13] T. Zhou, P. Nie, X. Cai, and P. K. Chu, “Influence of N2 partial pressure on mechanical properties of (Ti,Al)N films deposited by reactive magnetron sputtering,” *Vacuum*, vol. 83, no. 7, pp. 1057–1059, Mar. 2009, doi: 10.1016/j.vacuum.2009.01.001.

[14] F. Cai, S. Zhang, J. Li, Z. Chen, M. Li, and L. Wang, “Effect of nitrogen partial pressure on Al-Ti-N films deposited by arc ion plating,” *Appl Surf Sci*, vol. 258, no. 5, pp. 1819–1825, Dec. 2011, doi: 10.1016/j.apsusc.2011.10.053.

[15] F. Cai, M. Chen, M. Li, and S. Zhang, “Influence of negative bias voltage on microstructure and property of Al-Ti-N films deposited by multi-arc ion plating,” *Ceram Int*, vol. 43, no. 4, pp. 3774–3783, Mar. 2017, doi: 10.1016/j.ceramint.2016.12.019.

[16] C. Tian, H. Cai, and Y. Xue, “Effect of Working Pressure on Tribological Properties of Ce-Ti/MoS2 Coatings Using Magnetron Sputter,” *Coatings*, vol. 12, no. 10, Oct. 2022, doi: 10.3390/coatings12101576.

[17] B. Syed *et al.*, “Effect of varying N2pressure on DC arc plasma properties and microstructure of TiAlN coatings,” *Plasma Sources Sci Technol*, vol. 29, no. 9, Sep. 2020, doi: 10.1088/1361-6595/abaeb4.

[18] B. Warcholinski and A. Gilewicz, “Effect of substrate bias voltage on the properties of CrCN and CrN coatings deposited by cathodic arc evaporation”, doi: 10.1016/j.vacuum.2012.04.039.

[19] F. Cai, M. Chen, M. Li, and S. Zhang, “Influence of negative bias voltage on microstructure and property of Al-Ti-N films deposited by multi-arc ion plating,” 2016, doi: 10.1016/j.ceramint.2016.12.019.

[20] “Tool Wear: Meaning, Types and Causes | Metal Cutting.” https://www.yourarticlelibrary.com/metallurgy/tool-wear-meaning-types-and-causes-metal-cutting/96116 (accessed Aug. 07, 2022).

[21] B. Bhushan, “ Principles and Applications of Tribology19991 Principles and Applications of Tribology . USA: John Wiley & Sons Inc. 1999. , ISBN: 0 471 59407 5 US $150 ,” *Industrial Lubrication and Tribology*, vol. 51, no. 6, pp. 313–313, Dec. 1999, doi: 10.1108/ILT.1999.51.6.313.1.

[22] *Modern Metal Cutting, A Practical Handbook. Sandvik Coromant*.

[23] A. C. A. De Melo, J. C. G. Milan, M. B. Da Silva, and Á. R. Machado, “Some observations on wear and damages in cemented carbide tools,” *Journal of*

the Brazilian Society of Mechanical Sciences and Engineering, vol. 28, no. 3, pp. 269–277, 2006, doi: 10.1590/S1678-58782006000300004.

[24] "ISO - ISO 3685:1993 - Tool-life testing with single-point turning tools." https://www.iso.org/standard/9151.html (accessed Aug. 07, 2022).

[25] D. Philip Selvaraj, P. Chandramohan, and M. Mohanraj, "Optimization of surface roughness, cutting force and tool wear of nitrogen alloyed duplex stainless steel in a dry turning process using Taguchi method," *Measurement*, vol. 49, no. 1, pp. 205–215, Mar. 2014, doi: 10.1016/J.MEASUREMENT.2013.11.037.

[26] "Scheme of the Metaplas Ionon MZR 323 arc evaporation PVD system.... | Download Scientific Diagram." https://www.researchgate.net/figure/Scheme-of-the-Metaplas-Ionon-MZR-323-arc-evaporation-PVD-system-Courtesy-of-AIN_fig4_328963442 (accessed Sep. 04, 2023).

[27] K. D. Bouzakis, N. Michailidis, G. Skordaris, E. Bouzakis, D. Biermann, and R. M'Saoubi, "Cutting with coated tools: Coating technologies, characterization methods and performance optimization," *CIRP Annals*, vol. 61, no. 2, pp. 703–723, Jan. 2012, doi: 10.1016/J.CIRP.2012.05.006.

[28] J. M. F. De Paiva *et al.*, "Frictional and wear performance of hard coatings during machining of superduplex stainless steel", doi: 10.1007/s00170-017-0141-4.

[29] G. S. Fox-Rabinovich and A. I. Kovalev, “Self-organization and structural adaptation during cutting and stamping operations,” *Self-Organization During Friction: Advanced Surface-Engineered Materials and Systems Design*, pp. 151–166, Jan. 2006, doi: 10.1201/9781420017861.SEC3.

[30] H. A. Jehn, “Multicomponent and multiphase hard coatings for tribological applications,” *Surf Coat Technol*, vol. 131, no. 1–3, pp. 433–440, Sep. 2000, doi: 10.1016/S0257-8972(00)00783-0.

[31] B. Biswas, Y. Purandare, A. Sugumaran, I. Khan, and P. E. Hovsepian, “Effect of chamber pressure on defect generation and their influence on corrosion and tribological properties of HIPIMS deposited CrN/NbN coatings,” *Surf Coat Technol*, vol. 336, pp. 84–91, Feb. 2018, doi: 10.1016/J.SURFCOAT.2017.08.021.

[32] K. Lukaszkowicz, A. Paradecka, and J. Wiśniewska, “Structure and properties of CrN/DLC coating deposited by PVD ARC-cathodes and PACVD technology,” 2013. [Online]. Available: www.archivesmse.org

[33] V. V. Merie, G. Negrea, and E. Modi, “The influence of substrate temperature on the tribo-mechanical properties of chromium nitride thin films,” in *IOP Conference Series: Materials Science and Engineering*, Institute of Physics Publishing, Sep. 2016. doi: 10.1088/1757-899X/147/1/012020.

[34] W. Yongqiang, Z. Xiaoya, J. Zhiqiang, and T. Xiubo, “Characterization and mechanical properties of TiN/TiAlN multilayer coatings with different

modulation periods," *International Journal of Advanced Manufacturing Technology*, vol. 96, no. 5–8, pp. 1677–1683, May 2018, doi: 10.1007/S00170-017-0832-X.

[35] S. N. Grigoriev, A. A. Vereschaka, S. V Fyodorov, N. N. Sitnikov, and A. D. Batako, "Comparative analysis of cutting properties and nature of wear of carbide cutting tools with multi-layered nano-structured and gradient coatings produced by using of various deposition methods".

[36] A. Di Schino and J. M. Kenny, "Grain size dependence of the fatigue behaviour of a ultrafine-grained AISI 304 stainless steel," *Mater Lett*, vol. 57, no. 21, pp. 3182–3185, Jul. 2003, doi: 10.1016/S0167-577X(03)00021-1.

[37] A. Biksa *et al.*, "Wear behavior of adaptive nano-multilayered AlTiN/MexN PVD coatings during machining of aerospace alloys," *Tribol Int*, vol. 43, no. 8, pp. 1491–1499, Aug. 2010, doi: 10.1016/J.TRIBOINT.2010.02.008.

[38] P. S. Bapat, P. D. Dhikale, S. M. Shinde, A. P. Kulkarni, and S. S. Chinchanikar, "A Numerical Model to Obtain Temperature Distribution During Hard Turning of AISI 52100 Steel," *Mater Today Proc*, vol. 2, no. 4–5, pp. 1907–1914, Jan. 2015, doi: 10.1016/J.MATPR.2015.07.150.

[39] I. Korkut, M. Kasap, I. Ciftci, and U. Seker, "Determination of optimum cutting parameters during machining of AISI 304 austenitic stainless steel," *Mater Des*, vol. 25, no. 4, pp. 303–305, Jun. 2004, doi: 10.1016/J.MATDES.2003.10.011.

[40] Z. Tekiner and S. Yeşilyurt, “Investigation of the cutting parameters depending on process sound during turning of AISI 304 austenitic stainless steel,” *Mater Des*, vol. 25, no. 6, pp. 507–513, Sep. 2004, doi: 10.1016/J.MATDES.2003.12.011.

[41] S. S. P. A. J. P. R. V Ingle, “Machining challenges in stainless steel – a review.” https://www.slideshare.net/ijariit/machining-challenges-in-stainless-steel-a-review (accessed Aug. 18, 2022).

[42] P. S. Bapat, P. D. Dhikale, S. M. Shinde, A. P. Kulkarni, and S. S. Chinchanikar, “A Numerical Model to Obtain Temperature Distribution During Hard Turning of AISI 52100 Steel,” *Mater Today Proc*, vol. 2, no. 4–5, pp. 1907–1914, Jan. 2015, doi: 10.1016/J.MATPR.2015.07.150.

[43] J. S. A. David A. Stephenson, “Metal Cutting Theory and Practice.” Accessed: Aug. 21, 2022. [Online]. Available: https://www.taylorfrancis.com/books/mono/10.1201/9781315373119/metal-cutting-theory-practice-david-stephenson-john-agapiou

[44] L. Jiang, H. Hanninen, J. Paro, and V. Kauppinen, “Active Wear and Failure Mechanisms of TiN-Coated High Speed Steel and TiN-Coated Cemented Carbide Tools When Machining Powder Metallurgically Made Stainless Steels”.

[45] W. Grzesik, *Advanced Machining Processes of Metallic Materials: Theory, Modelling, and Applications: Second Edition*. Elsevier Inc., 2016. Accessed:

Aug. 03, 2023. [Online]. Available: http://www.sciencedirect.com:5070/book/9780444637116/advanced-machining-processes-of-metallic-materials

[46] E. Dow. Whitney, *Ceramic cutting tools : materials, development, and performance*. Noyes Publications, 1994. Accessed: Aug. 03, 2023. [Online]. Available: http://www.sciencedirect.com:5070/book/9780815513551/ceramic-cutting-tools

[47] "Advances in Ceramic Matrix Composites," *Advances in Ceramic Matrix Composites*, 2018, doi: 10.1016/C2016-0-03477-0.

[48] Y. S. Ahmed, G. Fox-Rabinovich, J. M. Paiva, T. Wagg, and S. C. Veldhuis, "Effect of Built-Up Edge Formation during Stable State of Wear in AISI 304 Stainless Steel on Machining Performance and Surface Integrity of the Machined Part," *Materials*, vol. 10, no. 11, Oct. 2017, doi: 10.3390/MA10111230.

[49] M. A. Xavior and M. Adithan, "Determining the influence of cutting fluids on tool wear and surface roughness during turning of AISI 304 austenitic stainless steel," *J Mater Process Technol*, vol. 209, no. 2, pp. 900–909, Jan. 2009, doi: 10.1016/J.JMATPROTEC.2008.02.068.

[50] A. K. Sharma, A. K. Tiwari, and A. R. Dixit, "Effects of Minimum Quantity Lubrication (MQL) in machining processes using conventional and nanofluid

based cutting fluids: A comprehensive review," *J Clean Prod*, vol. 127, pp. 1–18, Jul. 2016, doi: 10.1016/J.JCLEPRO.2016.03.146.

[51] P. S. Sreejith and B. K. A. Ngoi, "Dry machining: Machining of the future," *J Mater Process Technol*, vol. 101, no. 1–3, pp. 287–291, Apr. 2000, doi: 10.1016/S0924-0136(00)00445-3.

[52] S. Zhang, J. F. Li, and Y. W. Wang, "Tool life and cutting forces in end milling Inconel 718 under dry and minimum quantity cooling lubrication cutting conditions," *J Clean Prod*, vol. 32, pp. 81–87, Sep. 2012, doi: 10.1016/J.JCLEPRO.2012.03.014.

[53] P. S. Dirviyam, D. P. Selvaraj, and P. Chandramohan, "Optimization of surface roughness of AISI 304 austenitic stainless steel in dry turning operation using Taguchi design method Solar Photovoltaic water pumping systems View project Aluminum Metal Matrix composites View project OPTIMIZATION OF SURFACE ROUGHNESS OF AISI 304 AUSTENITIC STAINLESS STEEL IN DRY TURNING OPERATION USING TAGUCHI DESIGN METHOD," 2010. [Online]. Available: https://www.researchgate.net/publication/49595866

[54] A. E. Diniz, Á. R. Machado, and J. G. Corrêa, "Tool wear mechanisms in the machining of steels and stainless steels," *International Journal of Advanced Manufacturing Technology*, vol. 87, no. 9–12, pp. 3157–3168, Dec. 2016, doi: 10.1007/S00170-016-8704-3/METRICS.

[55] A. I. Fernández-Abia, J. Barreiro, J. Fernández-Larrinoa, L. N. López de Lacalle, A. Fernández-Valdivielso, and O. M. Pereira, “Behaviour of PVD coatings in the turning of austenitic stainless steels,” *Procedia Eng*, vol. 63, pp. 133–141, 2013, doi: 10.1016/J.PROENG.2013.08.241.

[56] I. Ciftci, “Machining of austenitic stainless steels using CVD multi-layer coated cemented carbide tools,” *Tribol Int*, vol. 39, no. 6, pp. 565–569, Jun. 2006, doi: 10.1016/J.TRIBOINT.2005.05.005.

[57] M. C. Shaw, “Metal Cutting,” *Oxford University Press* , 2005. https://www.scribd.com/document/357102925/Shaw-Milton-C-Metal-Cutting-Principles-Oxford-University-Press-2005-pdf# (accessed May 02, 2023).

[58] A. S. Kuprin *et al.*, “Structural, mechanical and tribological properties of Cr-V-N coatings deposited by cathodic arc evaporation,” *Tribol Int*, vol. 165, p. 107246, Jan. 2022, doi: 10.1016/J.TRIBOINT.2021.107246.

[59] Q. He, J. M. DePaiva, J. Kohlscheen, B. D. Beake, and S. C. Veldhuis, “Study of wear performance and tribological characterization of AlTiN PVD coatings with different Al/Ti ratios during ultra-high speed turning of stainless steel 304,” *Int J Refract Metals Hard Mater*, vol. 96, p. 105488, Apr. 2021, doi: 10.1016/J.IJRMHM.2021.105488.

[60] S. Y. Qiu, C. W. Wu, C. G. Huang, Y. Ma, and H. B. Guo, “Microstructure Dependence of Effective Thermal Conductivity of EB-PVD TBCs,” *Materials*, vol. 14, no. 8, Apr. 2021, doi: 10.3390/MA14081838.

[61] A. Ganvir, S. Joshi, N. Markocsan, and R. Vassen, “Tailoring columnar microstructure of axial suspension plasma sprayed TBCs for superior thermal shock performance,” *Mater Des*, vol. 144, pp. 192–208, Apr. 2018, doi: 10.1016/J.MATDES.2018.02.011.

[62] Z. Fan *et al.*, “Influence of columnar grain microstructure on thermal shock resistance of laser re-melted ZrO2-7 wt.% Y2O3 coatings and their failure mechanism,” *Surf Coat Technol*, vol. 277, pp. 188–196, Sep. 2015, doi: 10.1016/J.SURFCOAT.2015.07.036.

[63] Q. Luo, D. B. Lewis, P. E. Hovsepian, and W. D. Münz, “Transmission electron microscopy and x-ray diffraction investigation of the microstructure of nanoscale multilayer TiAlN/VN grown by unbalanced magnetron deposition,” *J Mater Res*, vol. 19, no. 4, pp. 1093–1104, 2004, doi: 10.1557/JMR.2004.0143.

[64] A. G. Stamopoulos, K. I. Tserpes, P. Prucha, and D. Vavrik, “Evaluation of porosity effects on the mechanical properties of carbon fiber-reinforced plastic unidirectional laminates by X-ray computed tomography and mechanical testing”, doi: 10.1177/0021998315602049.

[65] C. Torres-Sanchez, F. R. A. Al Mushref, M. Norrito, K. Yendall, Y. Liu, and P. P. Conway, “The effect of pore size and porosity on mechanical properties and biological response of porous titanium scaffolds,” *Materials Science and Engineering: C*, vol. 77, pp. 219–228, Aug. 2017, doi: 10.1016/J.MSEC.2017.03.249.

[66] B. Bachchhav and H. Bagchi, “Effect of surface roughness on friction and lubrication regimes”, doi: 10.1016/j.matpr.2020.06.252.

[67] H. Aghajani Derazkola, E. Garcia, and A. Murillo-Marrodán, “Effects of tool–workpiece interfaces friction coefficient on power and energy consumption during the piercing phase of seamless tube production,” *Journal of Materials Research and Technology*, vol. 19, pp. 3172–3188, Jul. 2022, doi: 10.1016/J.JMRT.2022.06.071.

[68] F. R. Lamastra, F. Leonardi, R. Montanari, F. Casadei, T. Valente, and G. Gusmano, “X-ray residual stress analysis on CrN/Cr/CrN multilayer PVD coatings deposited on different steel substrates,” *Surf Coat Technol*, vol. 200, no. 22-23 SPEC. ISS., pp. 6172–6175, Jun. 2006, doi: 10.1016/j.surfcoat.2005.11.013.

[69] B. WARCHOLINSKI, A. GILEWICZ, A. S. KUPRIN, and I. V. KOLODIY, “Structure and properties of CrN coatings formed using cathodic arc evaporation in stationary system,” *Transactions of Nonferrous Metals Society*

of China (English Edition), vol. 29, no. 4, pp. 799–810, Apr. 2019, doi: 10.1016/S1003-6326(19)64990-3.

[70] M. S. I. Chowdhury, B. Bose, G. Fox-rabinovich, and S. C. Veldhuis, “Investigation of the wear performance of tib2 coated cutting tools during the machining of ti6al4v alloy,” *Materials*, vol. 14, no. 11, 2021, doi: 10.3390/ma14112799.

[71] S. Zhao, H. Ma, Z. Chen, and J. K. Lancaster, “The relationship between the wear of carbon brush materials and their elastic moduli You may also like Analysis of Factors Affecting the Working Performance of Brush slip ring system in Special Environment The relationship between the wear of carbon brush materials and their elastic moduli,” *British Journal of Applied Physics To cite this article: J K Lancaster*, vol. 14, p. 497, 1963.

[72] B. D. Beake, G. S. Fox-Rabinovich, S. C. Veldhuis, and S. R. Goodes, “Coating optimisation for high speed machining with advanced nanomechanical test methods,” *Surf Coat Technol*, vol. 203, no. 13, pp. 1919–1925, Mar. 2009, doi: 10.1016/J.SURFCOAT.2009.01.025.

[73] B. D. Beake, G. S. Fox-Rabinovich, S. C. Veldhuis, and S. R. Goodes, “Coating optimisation for high speed machining with advanced nanomechanical test methods,” *Surf Coat Technol*, vol. 203, pp. 1919–1925, 2009, doi: 10.1016/j.surfcoat.2009.01.025.

[74] M. S. I. Chowdhury *et al.*, “Wear performance investigation of PVD coated and uncoated carbide tools during high-speed machining of TiAl6V4 aerospace alloy,” *Wear*, vol. 446–447, Apr. 2020, doi: 10.1016/j.wear.2019.203168.

[75] X. Huang, I. Etsion, and T. Shao, “Effects of elastic modulus mismatch between coating and substrate on the friction and wear properties of TiN and TiAlN coating systems,” 2015, doi: 10.1016/j.wear.2015.05.016.